# NUMERICAL APPROXIMATION OF VISCOELASTIC FLUIDS∗

Louis Perrotti[1], Noel J. Walkington[1] and Daren Wang[1]

**Abstract.** Stable finite element schemes are developed for the solution of the equations modeling the flow of viscoelastic fluids. In contrast with classical statements of these equations, which introduce the stress as a primary variable, these schemes explicitly involve the deformation tensor and elastic energy. Energy estimates and existence of solutions to the discrete problem are established for schemes of arbitrary order without any restrictions on the time step, mesh size, or Weissenberg number. Convergence to smooth solutions is established for the classical Oldroyd–B fluid. Numerical experiments for two classical benchmark problems verify the robustness of this approach.

**Mathematics Subject Classification.** 65M60, 65M12, 76M10.

## 1. Introduction

Stable numerical numerical schemes are developed for systems of the form

$$\rho\dot{v} - \operatorname{div}\left(-pI + 2\mu_s D(v) + (\alpha + \beta)D\mathcal{W}(E)E^\top\right) = \rho f,$$
$$\operatorname{div}(v) = 0, \tag{1.1}$$
$$\dot{E} - \alpha(\nabla v)E - \beta(\nabla v)^\top E + \frac{1}{2\mu_p}D\mathcal{W}(E) = 0,$$

supplemented with appropriate initial and boundary conditions. These equations model the flow of a polymer solution where $v(t,x) \in \mathbb{R}^d$ denotes the velocity and $D(v) = (1/2)(\nabla v + (\nabla v)^\top)$ the symmetric part of its gradient, $p$ denotes the pressure, and $E(t,x) \in \mathbb{R}^{d\times d}$ is a deformation tensor that gives rise to the elastic response. The density $\rho$, solvent viscosity $\mu_s$, and polymer viscosity $\mu_p$, are positive constants, and the constants $\alpha$ and $\beta$ characterize the polymer–solvent interaction. The strain energy $\mathcal{W} : \mathbb{R}^{d\times d} \to \mathbb{R}$ is typically an isotropic frame indifferent function; in particular, $D\mathcal{W}(E)E^\top$ is symmetric, and $\mathcal{W}(E)$ should diverge to infinity when $|E| \to \infty$ and when $\det(E) \to 0$.

These equations specialize to classical models of viscoelasticity with Weissenberg number We $> 0$ when

$$\mathcal{W}(E) = (\mu_p/2\text{We})\left(|E|^2 - |I|^2 - \log(\det(E)^2)\right), \qquad D\mathcal{W}(E) = (\mu_p/\text{We})(E - E^{-\top}), \tag{1.2}$$

[1] Department of Mathematics, Carnegie Mellon University, Pittsburgh, PA 15213. USA. `noelw@andrew.cmu.edu`

in which case the Cauchy stress, $T_e = (\alpha + \beta)D\mathcal{W}(E)E^\top = (\alpha + \beta)(\mu_p/\text{We})(EE^\top - I)$, satisfies

$$\dot{T}_e - \alpha(\nabla v)T_e - \alpha T_e(\nabla v)^\top - \beta(\nabla v)^\top T_e - \beta T_e(\nabla v) + \frac{1}{\text{We}}T_e = (\alpha + \beta)^2 \frac{2\mu_p}{\text{We}}D(v).$$

Traditionally this equation is used in place of the third equation of (1.1).

The development of stable numerical schemes using the classical statement of this problem with very modest Weissenberg numbers is notoriously difficult, so much so that it has the appellation "high Weissenberg number problem" (HWNP) [26]. The energy estimate for equations (1.1) is obtained by adding the dot product of the momentum equation with $v$ to the Frobenious product of the equation for the deformation with $D\mathcal{W}(E)$ and integrating by parts to give

$$\frac{\mathrm{d}}{\mathrm{d}t}\int_\Omega \left((\rho/2)|v|^2 + \mathcal{W}(E)\right) + \int_\Omega \left(2\mu_s|D(v)|^2 + (1/2\mu_p)|D\mathcal{W}(E)|^2\right) = \int_\Omega (\rho f, v). \tag{1.3}$$

In general $D\mathcal{W}(E)$ is very nonlinear and/or singular, so in a numerical context is not an admissible test function for the discrete weak statement. Additional issues arise with formulations based upon classical statements of the problem. The energy estimate is only meaningful if $EE^\top = (\text{We}/((\alpha + \beta)\mu_p))T_e + I$ is positive definite, and this is unlikely when $T_e$ is approximated by polynomials.

Below we show that convexity properties of the strain energy, and monotonicity of its derivative, can be exploited to obtain estimates on the solution of equations (1.1) that are inherited by Galerkin approximations. Convex analysis also provides natural regularizations of singular functions such as the logarithm in equation (1.2). These ideas were used in [31] to develop stable and convergent numerical schemes for the Ericksen Leslie equations, which model the flow of nematic liquid crystals and have a similar structure to (1.1).

**Overview.** The remainder of the section includes a discussion of related results and a summary of notation used. Section 2 contains a terse derivation of (1.1) and verifies equivalence with the classical equations. In Section 3 stable numerical numerical schemes are constructed for the equations modeling the Oldroyd–B fluid. Existence of solutions for the discrete problem is then direct, and in Section 4 we establish convergence to classical solutions (when they exist). To eliminate an excess of technical detail the analysis is presented for the Oldroyd–B fluid with homogeneous Dirichlet boundary data. Section 5 discusses extensions to more general fluids and addresses the numerical implementation of non–homogeneous boundary data. Numerical examples are presented in Section 6 for two benchmark problems. These examples illustrate that the finite element approximations of the weak statement of equations (1.1) developed in Section 3 are insensitive to the magnitude of the Weissenberg number.

## 1.1. Related results

While the computational literature on the high Weissenberg number problem is vast, the source of the instability associated with the HWNP remains a point of debate since the mathematical theory for the underlying equations is incomplete. Existence of (weak) solutions to the equations remains an open problem, but partial results are available. Current results fall into the following categories; local-in-time solutions for initial value problems, global-in-time solutions for small perturbations of the rest state, and results on steady flows of slightly perturbed Newtonian flows. Reviews of classical existence results are available in [15,18,19,27]. More recently the existence of classical solutions for the Oldroyd-B model at infinite Weissenberg number with small initial data has been proven by Lin *et al.* [23], and global-in-time existence results for weak solutions to the corotational Jeffrey's model have been obtained by Lions and Masmoudi [24]. This latter model is obtained by selecting $\beta = -\alpha$ in the third equation of (1.1) so that only the skew part of the velocity gradient appears. Barrett and Boyaval proved global-in-time weak solutions for a regularized Oldroyd model by adding a dissipative term in the constitutive equation and truncating the conformation tensor in the momentum equation. After constructing finite element approximations to the regularized system, they prove convergence along sub–sequences to solutions of the regularized problem as the discretization parameters tend to zero [4].

A comprehensive review of the engineering approach, where various types of finite element and stabilization terms are proposed to circumvent the HWNP, is available in Owens and Phillips [26]. An overview of the mathematical motivation for the various schemes and formulations utilized may be found in the work of Renardy [27], and a survey of more recent developments is presented in [22]. In a series of papers Ervin *et al.* [8–11] established convergence of finite element schemes at optimal rates to classical (smooth) solutions of the equations for the Oldroyd–B fluid. In this work the streamwise upwind Petrov Galerkin (SUPG) method was used to stabilize the convective terms; however, the classical energy estimate was not established for their schemes. Instead, error estimates were developed to prove that the numerical solution was close to a smooth classical solution, and hence bounded provided the latter existed. A key step in their analysis combines error and inverse estimates to develop uniform bounds on the solution. These are required to control the nonlinear terms and we use similar arguments in Section 4 for the same purpose.

Fattal and Kupferman [13] conjectured the HWNP instability stems from using polynomials to approximate the exponential growth of the stress tensor in regions with a high rate of deformation or stagnation points. To circumvent this issue they used a change of variables that scale logarithmically; more importantly, the conformation tensor remains positive definite with this formulation. Their "log conformation representation" facilitated stable calculations with no apparent limit to the value of the Weissenberg number, but the accuracy of their results in regions of large stress and strong rotations was not clear [12,14].

Boyaval, Lelievre and Mangoubi constructed stable (free-energy-dissipative) schemes for schemes using the classical differential model for the stress, and established stability of Fattal and Kupferman's LCR formulation for an Oldroyd-B fluid [6]. Implicit Euler time stepping and piecewise constant finite element approximations for the stress were essential for their proofs, which use nonlinear functions of the solution as test functions. In [5] the same authors report that instabilities associated with HWNP and loss of positivity may persist depending upon how the the convective terms in the constitutive equation are approximated.

From a mathematical standpoint, one reason for the limited success to date is that traditional stability (energy) estimates require the conformation tensor to be positive definite. There is growing evidence to suggest the loss of positivity is a precursor to HWNP instability. Fattal and Kupferman guarantee positivity by introducing the logarithm of the conformation tensor as a primary variable and use the property that the exponential of any matrix is positive. An alternative approach is to write the conformation matrix as $B = EE^\top$ to determine an evolution equation, such as the third equation in (1.1), satisfied by $E$. This is the approach taken by Lozinski and Owens [25] and Balci *et al.* [3] who introduce a square root of the conformation tensor as a primary variable and derive an equation for its evolution (see (2.3) in the next section). A variation of this idea exploited in [22] is to construct a time stepping scheme for which the updates to the conformation tensor at each time step take the form $(\delta E)(\delta E)^\top$ so that it remains positive definite.

In [22] Lee, Xu and Zhang use semi-Lagrangian schemes so that structure preserving methods from ODE's [17] can be exploited to preserve the positive definite property of the conformation tensor. Using these ideas the stability and existence of discrete solutions is established for a scheme with implicit Euler time stepping and divergence free finite element spaces for the velocity. As in prior work, the semi-Lagrangian schemes in [22] require piecewise constant approximations of the conformation tensor, or the construction of special projections to effect similar properties for piecewise linear elements. Numerical experiments for the drag coefficient for flow past a cylinder show convergence under mesh refinement for Weissenberg numbers 0.1 and 0.5. Their values for the drag are consistent with literature for We $\leq 0.75$, and they report difficulties obtaining convergence for Weissenberg values larger than 1.0. One may conjecture that there may not be a stationary solution, or it may be unstable, for this choice of parameters. This would be consistent with the numerical results in Section 6 below.

## 1.2. Notation

Below $\Omega \subset \mathbb{R}^d$ will denote a bounded domain with Lipschitz boundary. Standard notation is adopted for the Lebesgue spaces, $L^p(\Omega)$, and the Sobolev space $H^1(\Omega)$. Solutions of evolution equations will be viewed as functions from $[0, T]$ into these spaces, and we adopt the usual notion, $L^2[0, T; H^1(\Omega)]$, $C[0, T; H^1(\Omega)]$,
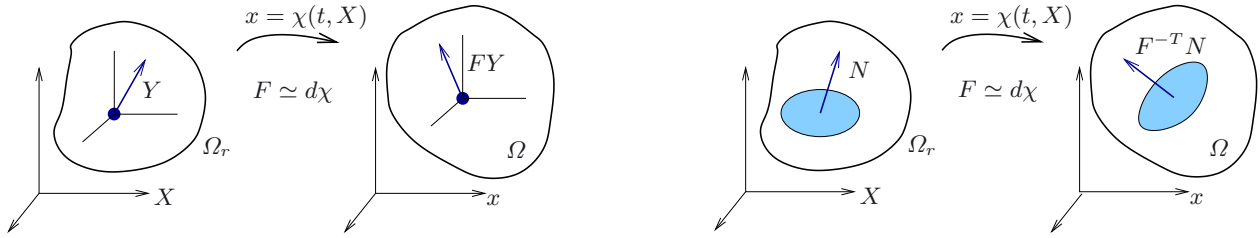
FIGURE 1. Transport of a fiber (*left*) and loop or disk (*right*).

*etc.* to indicate the temporal regularity. Divergences of vectors and matrices are denoted $\mathrm{div}(v) = v_{i,i}$ and $\mathrm{div}(T)_j = T_{ij,j}$ respectively. Here indices after the comma represent partial derivatives and the summation convention is used. Gradients of vector valued quantities are interpreted as matrices, $(\nabla v)_{ij} = v_{i,j}$, and the symmetric part of the velocity gradient is written as $D(u)$. Inner products are typically denoted as pairings $(.,.)$ or, for clarity, the dot product of two vectors $v, w \in \mathbb{R}^d$ may be written as $v.w = v_i w_i$ and the Frobenious inner product of two matrices $A, B \in \mathbb{R}^{d \times d}$ as $A : B = A_{ij} B_{ij}$.

Notation from continuum mechanics [16] is used in Section 2. In this section $X \in \Omega_r \subset \mathbb{R}^d$ denotes the Lagrangian coordinate and $x = \boldsymbol{\chi}(X,t)$ the Eulerian coordinate. The velocity is then $v(t,x) = \dot{x}(t,X)$; more generally, the convective time derivative is $\dot{g} = g_t + v.\nabla g$ where $\nabla$ denotes the gradient in the $x$ variables. The density in the reference configuration is denoted $\rho_r(X) > 0$ and its push forward under the flow map by $\rho(t,x)$. The incompressibility assumption on the fluid implies that $\rho_r$ and $\rho$ are constant.

## 2. VISCOELASTIC EQUATIONS

This section motivates the non–standard statement of the equations of viscoelasticity presented in equations (1.1), and can be read independently of the remainder of the paper.

Letting $E$ denote a measure of the strain (more precisely, the deformation) of a viscoelastic fluid, Hamilton's principle states that

$$\delta \int_{t_1}^{t_2} \int_{\Omega_r} \left( (1/2)|\dot{x}|^2 - \mathcal{W}(E) \right) \rho_r \, \mathrm{d}X \, \mathrm{d}t = \int_{t_1}^{t_2} \int_{\Omega(t)} \left( -(\rho f, \delta x) + (T_v, \nabla \delta x) \right) \, \mathrm{d}x \, \mathrm{d}t,$$

under (smooth compactly supported) variations of the flow map, $x \mapsto x + \delta x$. Here $T_v = 2\mu D(v)$ denotes the viscous component of the Cauchy stress and $\mathcal{W}(E)$ denotes the strain energy associated with the microstructural configuration. In order to compute the variation $\delta \mathcal{W}(E) = D\mathcal{W}(E) : \delta E$ it is necessary to specify the change of the deformation under to the variation $\delta x$. Classical elasticity assumes that $E$ responds like the Jacobian, $F$,

$$\delta F = \left[ \frac{\partial \delta x_i}{\partial X_\alpha} \right] = \left[ \frac{\partial \delta x_i}{\partial x_j} \frac{\partial x_j}{\partial X_\alpha} \right] = (\nabla \delta x) F,$$

which models stretching of material fibers, $Y \mapsto FY$ as illustrated in Figure 1. Different models of the microstructure give rise to different kinematics; for example, disk like particles in Stokes' flow with (non–unit) normal $n = EN$ satisfy $\delta n = -(\nabla \delta x)^\top EN$ [20]. The general expression

$$\delta E = \left( \alpha(\nabla \delta x) + \beta(\nabla \delta x)^\top \right) E, \tag{2.1}$$

assumed in equations (1.1) includes many of the classical viscoelastic models [21]. In this situation

$$\delta \int_{\Omega_r} W(E) \rho_r \, \mathrm{d}X = \int_{\Omega_r} \left( D\mathcal{W}(E), \alpha(\nabla \delta x)E + \beta(\nabla \delta x)^\top E \right) \rho_r \, \mathrm{d}X$$

$$= \int_{\Omega(t)} \left( (\alpha + \beta) D\mathcal{W}(E)E^\top, \nabla \delta x \right) \rho \, \mathrm{d}x,$$

where the last equality follows from the property that $D\mathcal{W}(E)E^\top$ is symmetric. The density is constant when the fluid is incompressible and is absorbed into the definition of $\mathcal{W}$.

The third equation in (1.1) is a gradient flow of the strain energy. Specifically, when $E$ is viewed as an element of the Lie group $GL_d(\mathbb{R})$, the term $\alpha(\nabla\delta x) + \beta(\nabla\delta x)^\top$ in equation (2.1) can be identified with an element of the Lie algebra, and the corresponding Lie derivative becomes

$$\mathring{E} \equiv \dot{E} - \alpha(\nabla v)E - \beta(\nabla v)^\top E.$$

When the polymer is passively transported $\mathring{E} = 0$, and non–zero values of $\mathring{E}$ model a mismatch between the fluid and polymer strain rates which gives rise to dissipation. A gradient flow, $\mathring{E} = -(1/2\mu_p)D\mathcal{W}(E)$, results when relaxation of the elastic stress is assumed to be the mechanism driving this mismatch back to equilibrium.

## 2.1. Equivalence with classical formulation

When the strain energy is given by equation (1.2), the conformation tensor $B \equiv (\alpha + \beta)^{-1}(\mathrm{We}/\mu_p)T_e + I = EE^\top$ satisfies

$$\dot{B} - \alpha(\nabla v)B - \alpha B(\nabla v)^\top - \beta(\nabla v)^\top B - \beta B(\nabla v) + \frac{1}{\mathrm{We}}B = \frac{1}{\mathrm{We}}I. \tag{2.2}$$

If $B(0)$ is symmetric positive definite, then so too is $B(t)$, and the following lemma shows that for any decomposition of the form $B = EE^\top$ the matrix $E$ satisfies

$$\dot{E} - EW - \alpha(\nabla v)E - \beta(\nabla v)^\top E + \frac{1}{2\mathrm{We}}\left(E - E^{-\top}\right) = 0 \tag{2.3}$$

for some skew matrix $W$; a similar result appears in [3].

**Lemma 2.1.** *Let $v \in C[0, T; C^1(\Omega)^d]$ and vanish on $\partial\Omega$.*

(1) *Let $E \in C^1[0, T; \mathbb{R}^{d\times d}]$ be invertible and satisfy equation (2.3) for some $W \in C[0, T; \mathbb{R}^{d\times d}_{skw}]$, then $B \equiv EE^\top$ satisfies (2.2).*
(2) *Let $B \in C^1[0, T; \mathbb{R}^{d\times d}_{sym}]$ be symmetric positive definite and satisfy equation (2.2). If $B = EE^\top$ with $E \in C^1[0, T; \mathbb{R}^{d\times d}]$, then there exists $W \in C[0, T; \mathbb{R}^{d\times d}_{skw}]$ such that $E$ satisfies (2.3). Moreover, there exists a decomposition $B = EE^\top$ with $E \in C^1[0, T; \mathbb{R}^{d\times d}]$ such that equation (2.3) holds with $W = 0$.*

*Proof.*

(1) Using equation (2.3) to eliminate $\dot{E}$ from the identity $\dot{B} = \dot{E}E^\top + E\dot{E}^\top$ shows $EE^\top$ satisfies (2.2).
(2) Substituting $B = EE^\top$ into equation (2.2) shows

$$(2.3)_0\, E^\top + E\, (2.3)_0^\top = 0,$$

where $(2.3)_0$ denotes equation (2.3) with $W = 0$. It follows that $(2.3)_0\, E^\top$ is skew, and equation (2.3) follows upon setting $(2.3)_0\, E^\top = EWE^\top$.
To eliminate $W$, let $B = \tilde{E}\tilde{E}^\top$ be any splitting of $B$ (for example, the SPD square root), and let $W$ be the corresponding skew matrix. Then $E = \tilde{E}Q$ satisfies $(2.3)_0$ when $Q$ is selected to be the orthogonal matrix satisfying $\dot{Q} = WQ$ with $Q(0) = I$. $\qquad\square$

## 2.2. Example: Poiseuille flow

In two dimensions the triple $(v, p, T_e)$ with

$$v = \begin{pmatrix} \frac{1}{2}(h^2 - y^2) \\ 0 \end{pmatrix}, \qquad p = -x, \qquad T_e = \begin{bmatrix} 2\mathrm{We}\mu_p y^2 & -\mu_p y \\ -\mu_p y & 0 \end{bmatrix}, \qquad (x, y) \in \mathbb{R}^2,$$

is a solution of the equations governing the flow of an Oldroyd-B fluid with parameters $\alpha = 1$ and $\beta = 0$ and boundary conditions $v(\pm h) = 0$.

- The pair

$$\tilde{E} = \begin{bmatrix} \sqrt{\mathrm{We}^2 y^2 + 1} & -\mathrm{We}y \\ 0 & 1 \end{bmatrix}, \quad \text{and} \quad W = \begin{bmatrix} 0 & \frac{1}{2}\frac{y}{\sqrt{\mathrm{We}^2 y^2 + 1}} \\ -\frac{1}{2}\frac{y}{\sqrt{\mathrm{We}^2 y^2 + 1}} & 0 \end{bmatrix},$$

  is the steady solution of equation (2.3) with $\tilde{E}$ upper triangular for which $\tilde{E}\tilde{E}^{\top} = (\mathrm{We}/\mu_p)T_e + I$.
- The splitting $EE^{\top} = (\mathrm{We}/\mu_p)T_e + I$ satisfying equation (2.3) with $W = 0$ is $E = \tilde{E}Q$ where $Q = Q(t,x,y)$ is the orthogonal matrix

$$Q = \begin{bmatrix} \cos(\theta) & -\sin(\theta) \\ \sin(\theta) & \cos(\theta) \end{bmatrix}, \quad \text{with} \quad \theta(t,x,y) = \omega(y)t + \theta_0\left(x - v(y)t, y\right).$$

Here $\theta_0(x,y) = \theta(0,x,y)$ is the initial value and

$$v(y) = \frac{h^2 - y^2}{2} \quad \text{and} \quad \omega(y) = \frac{y}{2\sqrt{\mathrm{We}^2 y^2 + 1}}.$$

This solution is independent of time if $\theta_0(x,y) = \left(\omega(y)/v(y)\right)x + C$; however, $v(\pm h) = 0$ so this function diverges at $y = \pm h$.

## 3. Numerical approximation

We consider the classical viscoelastic fluids for which the strain energy takes the form shown in equation (1.2), and without loss of generality set $\rho = 1$. In this situation a classical solution of equations (1.1) satisfies the weak statement

$$\int_{\Omega}\left\{(\dot{v},w) - (p,\mathrm{div}(w)) + 2\mu_s(D(v),D(w)) + \frac{\mu_p}{\mathrm{We}}(EE^T - I, \alpha\nabla w + \beta(\nabla w)^T)\right\} = \int_{\Omega}(f,w),$$

$$\int_{\Omega}(\mathrm{div}(v),q) = 0 \tag{3.1}$$

$$\int_{\Omega}\left(\dot{E} - \alpha(\nabla v)E - \beta(\nabla v)^{\top}E + \frac{1}{2\mathrm{We}}(E - E^{-\top}), G\right) = 0,$$

for all smooth test functions $(w,q,G)$ with $w$ vanishing on the boundary. Below the term

$$(I, \alpha\nabla w + \beta(\nabla w)^{\top}) = (\alpha + \beta)\mathrm{div}(w)$$

will be absorbed into the pressure. Setting $(w,q,G) = (v,p,(\mu_p/\mathrm{We})E)$ shows

$$\frac{\mathrm{d}}{\mathrm{d}t}\int_{\Omega}\frac{1}{2}\left(|v|^2 + \frac{\mu_p}{\mathrm{We}}|E|^2\right) + \int_{\Omega}\left(2\mu_s|D(v)|^2 + \frac{\mu_p}{2\mathrm{We}^2}|E|^2\right) = \int_{\Omega}\left((f,v) + \frac{\mu_p}{2\mathrm{We}^2}|I|^2\right).$$

The bounds from this expression are not as sharp as those available from the classical energy balance (1.3); however, unlike the energy balance they are inherited by Galerkin approximations of (3.1).

### 3.1. Numerical scheme

Let $0 = t^0 < t^1 < \ldots < t^N = T$ be a partition of $[0,T]$ and $\mathcal{T}_h$ be a triangulation of the domain $\Omega$. On each interval of the partition approximate solutions $(v_h, p_h, E_h)$ of equations (1.1) will take values in the spaces

$$\mathcal{P}_{\ell}[t^{n-1}, t^n; \mathbb{V}_h] \times \mathcal{P}_{\ell}[t^{n-1}, t^n; \mathbb{P}_h] \times \mathcal{P}_{\ell}[t^{n-1}, t^n; \mathbb{E}_h], \tag{3.2}$$

where $(\mathbb{V}_h, \mathbb{P}_h) \subset H_0^1(\Omega)^d \times L^2(\Omega)/\mathbb{R}$ is a div–stable finite element pair and $\mathbb{E}_h \subset L^2(\Omega)^{d \times d}$. While it is not necessary for the temporal dependence of $E_h$ to have the same degree as $(v_h, p_h)$, there is no reason for it not to.

Since $E_h^{-\top}$ does not exist for every $E_h \in \mathbb{E}_h$ it is necessary to regularize this term. Solutions of $(1.1)_3$ have non–negative determinant, thus if $\det_\epsilon(E)$ denotes a non–negative approximation of $\det(E)$, a natural approximation of the inverse transpose is

$$E_\epsilon^{-\top} \equiv \frac{1}{\det_\epsilon(E)}\text{Cof}(E) \quad \text{so that} \quad (E_\epsilon^{-\top}, E) = d\frac{\det(E)}{\det_\epsilon(E)},$$

where $\text{Cof}(E) \simeq \det(E)E^{-\top}$ denotes the matrix of cofactors of $E$. Below we construct regularizations which penalize negative determinants,

$$\lim_{\epsilon \to 0} \frac{\det(E)}{\det_\epsilon(E)} = 1 \text{ when } \det(E) > 0 \quad \text{and} \quad \lim_{\epsilon \to 0} \frac{\det(E)}{\det_\epsilon(E)} = -\infty \text{ when } \det(E) < 0. \tag{3.3}$$

The discontinuous Galerkin methodology will be used to construct stable approximations of the transport terms and time derivatives. We adopt the standard notation for the jump terms that arise.

- Superscripts will be used to denote function values at the partition points, $v_{h\pm}^n = v_h(t_\pm^n)$ with jumps denoted analogously,
$$[v_h]^n = v_h(t_+^n) - v_h(t_-^n) \qquad [E_h]^n = E_h(t_+^n) - E_h(t_-^n).$$

- If $K \in \mathcal{T}_h$ and $x \in \partial K$ then $E_{h\pm}(x) = \lim_{s \to 0_+} E_h(x \pm sn)$, where $n$ is the outward normal vector on $\partial K$. If $F = K_+ \cap K_-$ is a face in $\mathcal{T}_h$ the jump of $E_h$ across $F$ is denoted $[E_h]$; terms involving the spatial jumps will be paired so that their value is independent of the choice of face normal.

- If $a \in \mathbb{R}$ then $a^- = \max\{0, -a\}$ denotes the negative part of $a$ and $a^+ = \max\{0, a\}$ the positive part.

On each temporal partition the numerical scheme to approximate solutions of equations $(1.1)$ seeks

$$(v_h, p_h, E_h) \in \mathcal{P}_\ell[t^{n-1}, t^n; \mathbb{V}_h] \times \mathcal{P}_\ell[t^{n-1}, t^n; \mathbb{P}_h] \times \mathcal{P}_\ell[t^{n-1}, t^n; \mathbb{E}_h].$$

satisfying

$$\int_{t^{n-1}}^{t^n} \int_\Omega \left\{ (v_{ht}, w_h) + \frac{1}{2}((v_h.\nabla)v_h, w_h) - \frac{1}{2}((v_h.\nabla)w_h, v_h) - (p_h, \text{div}(w_h)) + (2\mu_s D(v_h), D(w_h)) \right.$$
$$\left. + \frac{\mu_p}{\text{We}} \left( E_h E_h^T, \alpha\nabla w_h + \beta(\nabla w_h)^T \right) \right\} + \int_\Omega ([v_h]^{n-1}, w_h(t_+^{n-1})) = \int_0^T \int_\Omega (f, w_h),$$

$$\int_{t^{n-1}}^{t^n} \int_\Omega (\text{div}(v_h), q_h) = 0, \tag{3.4}$$

$$\int_{t^{n-1}}^{t^n} \left\{ \int_\Omega (\dot{E} - \alpha(\nabla v_h)E_h - \beta(\nabla v_h)^\top E_h, G_h) + \frac{1}{2}\text{div}(v_h)(E_h, G_h) + \frac{1}{2\text{We}}(E_h - E_{h\epsilon}^{-T}), G_h) \right.$$
$$\left. + \sum_{K \in \mathcal{T}_h} \int_{\partial K} (v_h \cdot n)^-([E_h], G_{h-}) \right\} + \int_\Omega ([E_h^{n-1}], G_h(t_+^{n-1})) = 0,$$

for all

$$(w_h, q_h, G_h) \in \mathcal{P}_\ell[t^{n-1}, t^n; \mathbb{V}_h] \times \mathcal{P}_\ell[t^{n-1}, t^n; \mathbb{P}_h] \times \mathcal{P}_\ell[t^{n-1}, t^n; \mathbb{E}_h].$$

## 3.2. Existence and stability

The following notation is adopted for the terms appearing in the weak statement.

- The bilinear dissipative term is

$$a((v_h, E_h), (w_h, G_h)) = \int_\Omega 2\mu_s(D(v_h), D(w_h)) + \frac{\mu_p}{2\text{We}^2}(E_h, G_h).$$

- The trilinear terms in the weak statement are

$$c((u, E), (v, F), (w, G)) = \sum_{K \in \mathcal{T}_h} \int_K \left\{ \frac{1}{2}((u \cdot \nabla)v, w) - \frac{1}{2}((u \cdot \nabla)w, v) \right.$$

$$+ \frac{\mu_p}{\text{We}} \left( \alpha(F, \nabla w\, E) - \alpha(G, \nabla v\, E) + \beta(F, (\nabla w)^T E) - \beta(G, (\nabla v)^T E) \right)$$

$$+ \left. \frac{\mu_p}{\text{We}}((u \cdot \nabla)F, G) + \frac{\mu_p}{2\text{We}}\text{div}(u)(F, G) \right\}.$$

- The jump term is

$$J_h(u, F, G) = \frac{\mu_p}{\text{We}} \sum_{K \in \mathcal{T}_h} \int_{\partial K} (u.n)^-([F], G).$$

This form of the trilinear term was chosen so that only the matrix $F$ in the second argument of $c(.,.,.)$ is differentiated. In place of the usual skew symmetry we have the identity

$$c((u, E), (v, F), (v, F)) + J_h(u, F, F) = \frac{\mu_p}{2\text{We}} \sum_{e \in \mathcal{T}_h^{d-1}} \int_e |u.n|\, |[F]|^2,$$

where $\mathcal{T}_h^{d-1}$ denotes the interior edges/faces of $\mathcal{T}_h$. Using this notation the discrete weak statement (3.4) can be written as

$$\int_{t^{n-1}}^{t^n} \left\{ (v_{ht}, w_h) + \frac{\mu_p}{\text{We}}(E_{ht}, G_h) + a((v_h, E_h), (w_h, G_h)) - (p_h, \text{div}(w_h)) + (q_h, \text{div}(v_h)) \right.$$

$$\left. + c((v_h, E_h), (v_h, E_h), (w_h, G_h)) + J_h(v_h, E_h, G_h) \right\} + \left( [v_h]^{n-1}, w_h(t_+^{n-1}) \right) \tag{3.5}$$

$$+ \frac{\mu_p}{\text{We}}\left( [E_h]^{n-1}, G_h(t_+^{n-1}) \right) = \int_{t^{n-1}}^{t^n} \left\{ (f, w_h) + \frac{\mu_p}{2\text{We}^2}(E_{h\epsilon}^{-T}, G_h) \right\},$$

where $(.,.)$ denotes an $L^2(\Omega)$ pairing. Setting $(w_h, q_h, G_h) = (v_h, p_h, E_h)$ and summing gives the stability estimate

$$\|v_{h-}^n\|_{L^2(\Omega)}^2 + \frac{\mu_p}{\text{We}}\|E_{h-}^n\|_{L^2(\Omega)}^2 + \sum_{m=0}^{n-1} \left( \|[v_h]^m\|_{L^2(\Omega)}^2 + \frac{\mu_p}{\text{We}}\|[E_h]^m\|_{L^2(\Omega)} \right)$$

$$+ \int_0^{t^n} \left\{ 2\mu_s\|D(v_h)\|_{L^2(\Omega)}^2 + \frac{\mu_p}{\text{We}^2}\|E_h\|_{L^2(\Omega)}^2 + 2d\|\det(E_h)^-/\det_\epsilon(E_h)\|_{L^1(\Omega)} \right\} \tag{3.6}$$

$$+ \frac{\mu_p}{\text{We}} \sum_{F \in \mathcal{T}_h^{d-1}} \int_0^{t^n} \int_F |v_h \cdot n|\, [E_h]^2 \leq \|v_{h-}^0\|_{L^2(\Omega)}^2 + \frac{\mu_p}{\text{We}}\|E_{h-}^0\|_{L^2(\Omega)}^2 + \frac{1}{\mu_s}\int_0^{t^n}\|f\|_{H^{-1}(\Omega)}^2 + \frac{\mu_p}{2\text{We}^2}d|\Omega|t^n.$$

where it was assumed that $\det(E)/\det_\epsilon(E_h) \leq 1$.

**Theorem 3.1.** *Let $\alpha$, $\beta \in \mathbb{R}$, $\mu_s$, $\mu_p > 0$, and $f \in L^2[t^{n-1}, t^n; H^{-1}(\Omega)]$. Let $\mathbb{V}_h \times \mathbb{P}_h \subset H_0^1(\Omega)^d \times L^2(\Omega)/\mathbb{R}$ be a div–stable pair of finite dimensional subspaces and let $\mathbb{E}_h \subset L^2(\Omega)^{d \times d}$ be a finite dimensional subspace. Let $E_h \mapsto \det(E_h)/\det_\epsilon(E_h) \in (-\infty, 1]$ be continuous on $\mathbb{E}_h$ and set $E_{\epsilon h}^{-\top} = (1/\det_\epsilon(E_h))\mathrm{Cof}(E_h)$. Then for each $t^{n-1} < t^n$ and $(v_{h-}^{n-1}, E_{h-}^{n-1}) \in \mathbb{V}_h \times \mathbb{E}_h$ there exists a triple*

$$(v_h, p_h, E_h) \in \mathcal{P}_\ell[t^{n-1}, t^n; \mathbb{V}_h] \times \mathcal{P}_\ell[t^{n-1}, t^n; \mathbb{P}_h] \times \mathcal{P}_\ell[t^{n-1}, t^n; \mathbb{E}_h],$$

*satisfying (3.4).*

*Proof.* Let $\mathbb{Z}_h = \{v_h \in \mathbb{V}_h \mid (\mathrm{div}(v_h), p_h) = 0, \; p_h \in \mathbb{P}_h\}$ denote the discretely divergence free subspace and $\Phi_h : \mathcal{P}_\ell[t^{n-1}, t^n; \mathbb{Z}_h \times \mathbb{E}_h] \to \mathcal{P}_\ell[t^{n-1}, t^n; \mathbb{Z}_h \times \mathbb{E}_h]$ be characterized by

$$\Phi_h(v_h, E_h) \cdot (w_h, G_h) = \int_{t^{n-1}}^{t^n} \left\{ (v_{ht}, w_h) + \frac{\mu_p}{\mathrm{We}}(E_{ht}, G_{ht}) + a((v_h, E_h), (w_h, G_h)) \right.$$

$$+ c((v_h, E_h), (v_h, E_h), (w_h, G_h)) + J_h(v_h, E_h, G_h) - (f, w_h) - \left. \frac{\mu_p}{2\mathrm{We}^2}(E_{h\epsilon}^{-T}, G_h) \right\}$$

$$+ ([v_h]^{n-1}, w_h(t_+^{n-1})) + \frac{\mu_p}{\mathrm{We}}([E_h]^{n-1}, G_h(t_+^{n-1})),$$

where the dot on the left denotes an inner product on $\mathcal{P}_\ell[t^{n-1}, t^n; \mathbb{Z}_h \times \mathbb{E}_h]$. The stability estimate guarantees

$$\Phi_h(v_h, E_h) \cdot (v_h, E_h) = \frac{1}{2}\left( \|v_h(t_-^n)\|_{L^2(\Omega)}^2 + \frac{\mu_p}{\mathrm{We}}\|E_h(t_-^n)\|_{L^2(\Omega)}^2 \right)$$

$$+ \frac{1}{2}\left( \|[v_h]^{n-1}\|_{L^2(\Omega)}^2 + \frac{\mu_p}{\mathrm{We}}\|[E_h]^{n-1}\|_{L^2(\Omega)}^2 \right)$$

$$+ \int_{t^{n-1}}^{t^n} \left\{ 2\mu_s \|D(v_h)\|_{L^2(\Omega)}^2 + \frac{\mu_p}{2\mathrm{We}^2}\|E_h\|_{L^2(\Omega)}^2 + \frac{\mu_p}{2\mathrm{We}} \sum_{F \in \mathcal{T}_h^{d-1}} \int_F |v_h \cdot n| \, [E_h]^2 \right\}$$

$$- \frac{1}{2}\left( \|v_h(t_-^{n-1})\|_{L^2(\Omega)}^2 + \frac{\mu_p}{\mathrm{We}}\|E_h(t_-^{n-1})\|_{L^2(\Omega)}^2 \right)$$

$$- \int_{t^{n-1}}^{t^n} \left\{ (f, v_h) + \frac{\mu_p}{2\mathrm{We}^2}(E_{h\epsilon}^{-T}, E_h) \right\}.$$

The Brouwer fixed point theorem guarantees that $\Phi_h$ has a zero if the right hand side is positive when $(v_h, E_h)$ is sufficiently large ([28], Prop. II.2.1), which is the case since the last term is bounded below by $-(\mu_p/2\mathrm{We}^2)d|\Omega|$. The existence of a pressure then follows from the assumption that the pair $(\mathbb{V}_h, \mathbb{P}_h)$ is div–stable. $\qquad\square$

## 3.3. Regularizations of the determinant

To complete the specification of a numerical schemes it is necessary to select a regularization of the (reciprocal of the) determinant. Since the term $E^{-\top}$ arises as the derivative of the logarithm of the determinant, and the map $x \mapsto -\ln(x)$ is convex on $(0, \infty)$, it is natural to consider the Yosida approximation

$$\frac{1}{\det_\epsilon(E)} = \frac{2}{\sqrt{\det(E)^2 + 4\epsilon^2} + \det(E)}. \tag{3.7}$$

The convergence proof below requires $E_\epsilon^{-\top}$ to be bounded which can be achieved by the following modification of the Yosida approximation;

$$\frac{1}{\det_\epsilon(E)} = \frac{2}{\sqrt{\det(E)^2 + 4\epsilon^2 + \epsilon^2|E|^{2(d-1)}} + \det(E)}. \tag{3.8}$$

With this choice $\det(E)/\det_\epsilon(E) \leq 1$ and $E_\epsilon^{-\top} = (1/\det_\epsilon(E))\mathrm{Cof}(E)$ is bounded by a constant of the form $C(d)/\epsilon$. Lipschitz continuity and approximation properties of this regularization are developed in Lemma 4.4 below.

To verify that this approximation penalizes negative values of the determinant, suppose $\det(E) < 0$ and write $\delta = -\det(E)$ and $e = |E|$. Then

$$\frac{-\det(E)}{\det_\epsilon(E)} = \frac{2\delta}{\sqrt{\delta^2 + (4 + e^{2(d-1)})\epsilon^2} - \delta} = \frac{2\delta(\sqrt{\delta^2 + (4 + e^{2(d-1)})\epsilon^2} + \delta)}{(4 + e^{2(d-1)})\epsilon^2} \geq \frac{2\delta^2}{(4 + e^{2(d-1)})\epsilon^2},$$

and

$$\frac{2\delta}{\epsilon} = \frac{2\delta}{(2 + e^{d-1})\epsilon}(2 + e^{d-1}) \leq \frac{\delta^2}{(2 + e^{d-1})^2\epsilon^2} + (2 + e^{d-1})^2.$$

It follows that there exists a constant $C = C(d)$ such that

$$\det(E)^- \leq C\left(1 + |\det(E)^-/\det_\epsilon(E)| + |E|^2\right)\epsilon, \qquad\qquad d = 2,$$
$$\sqrt{\det(E)^-} \leq C\left(1 + |\det(E)^-/\det_\epsilon(E)| + |E|^2\right)\sqrt{\epsilon}, \qquad\qquad d = 3.$$

Equation (3.6) bounds right hand side of these expressions for the deformation of the discrete solution so

$$\|(\det(E_h)^-)^{1/(d-1)}\|_{L^1[0,T;L^1(\Omega)]} \leq C\epsilon^{1/(d-1)}.$$

## 4. Convergence

In this section convergence is established for solutions of the numerical scheme (3.5) to a classical solutions of equations (1.1) with the classical elastic energy (1.2). To reduce the technical detail we focus on the practically important case of a second order scheme in space and time with maximal time step $\tau$ and mesh parameter $h$ of similar size, $c \leq h/\tau \leq C$. Equation (3.8) will be used to regularize the (reciprocal of the) determinant of $E$ with regularization parameter $\epsilon$ comparable to the mesh size, $c \leq \epsilon/(\tau \ln(1/\tau)) \leq C$. With this choice of parameters we establish the essentially optimal second order rate of convergence.

The Galerkin orthogonality condition for the error follows upon restricting the test functions in equation (3.1) to the finite element spaces and subtracting equation (3.5);

$$\int_{t^{n-1}}^{t^n} \left\{ (v_t - v_{ht}, w_h) + \frac{\mu_p}{\mathrm{We}}(E_t - E_{ht}, G_h) - (p - p_h, \mathrm{div}(w_h)) + a((v - v_h, E - E_h), (w_h, G_h)) \right.$$
$$\left. + c((v,E),(v,E),(w_h,G_h)) - c((v_h,E_h)(v_h,E_h),(w_h,G_h)) - J_h(v_h,E_h,G_h) \right\}$$
$$- ([v_h], w_{h+})^{n-1} - \frac{\mu_p}{\mathrm{We}}([E_h], G_{h+})^{n-1} = \int_{t^{n-1}}^{t^n} \frac{\mu_p}{2\mathrm{We}^2}(E^{-T} - E_{h\epsilon}^{-T}, G_h), \quad (4.1)$$

for all $(w_h, G_h) \in \mathcal{P}_\ell[t^{n-1}, t^n; \mathbb{V}_h \times \mathbb{E}_h]$. The error $(v - v_h, E - E_h)$ will be decomposed into the sum of a projection error and consistency error,

$$(v - v_h, E - E_h) = (v - v_p, E - E_p) + (v_p - v_h, E_p - E_h) \equiv (e_p, \mathcal{E}_p) + (e_h, \mathcal{E}_h),$$

where $(v_p, E_p) \in \mathcal{P}_\ell[t^{n-1}, t^n; \mathbb{V}_h \times \mathbb{E}_h]$ is a projection or interpolant of $(v, E)$ into the finite element spaces. The orthogonality condition is then used to bound the consistency error by the projection error thereby establishing convergence at the optimal rates when the solution is smooth. While any reasonable projection can be utilized, the following choice simplifies the analysis DG approximations of the temporal terms.

**Definition 4.1.** The projection

$$\mathbb{P}_h^n : C\left[t^{n-1}, t^n; L^2(\Omega)^d \times L^2(\Omega)^{d\times d}\right] \to \mathcal{P}_\ell\left[t^{n-1}, t^n; \mathbb{V}_h \times \mathbb{E}_h\right]$$

is characterized as

$$\mathbb{P}_h^n(v, E) = \left(\mathbb{P}^n \circ P_{\mathbb{Z}_h}(v), \mathbb{P}^n \circ P_{\mathbb{E}_h}(E)\right),$$

with spatial projections

- $P_{\mathbb{Z}_h} : L^2(\Omega)^d \to \mathbb{Z}_h \subset \mathbb{V}_h$ the $L^2$-orthogonal projection onto the discretely divergence free subspace of $\mathbb{V}_h$,

$$\mathbb{Z}_h = \{v_h \in \mathbb{V}_h \mid (\mathrm{div}(v_h), q_h) = 0, \ q_h \in \mathbb{P}_h\},$$

- $P_{\mathbb{E}_h} : L^2(\Omega)^{d\times d} \to \mathbb{E}_h$ the orthogonal projection,

and for any Banach space $W$ the temporal projection $\mathbb{P}^n : C[t^{n-1}, t^n; W] \to \mathcal{P}_\ell[t^{n-1}, t^n; W]$ is characterized by $\mathbb{P}^n(w)(t_-^n) = w(t^n)$ and

$$\int_{t^{n-1}}^{t^n} (\mathbb{P}^n(w) - w)\phi = 0, \qquad \phi \in \mathcal{P}_{\ell-1}(t^{n-1}, t^n).$$

For the classical finite element spaces, this projection exhibits optimal rates of convergence in $H_0^1(\Omega)^d \times L^2(\Omega)^{d\times d}$ and the spatial and temporal projections commute, so $\mathbb{P}_h^n(v, E) = (P_{\mathbb{Z}_h} \circ \mathbb{P}^n(v), P_{\mathbb{E}_h} \circ \mathbb{P}^n(E))$.

**Theorem 4.2.** *$\Omega \subset \mathbb{R}^d$ bounded Lipschitz domain, $T > 0$, and let $\{\mathcal{T}_h\}_{h>0}$ be a quasi–uniform family of triangulations of $\Omega$ and $\{t_h^n\}_{n=0}^{N_h}$ a family of quasi–uniform partitions of $[0, T]$. Assume that there exist constants $0 < c < C$ such that the spatial and temporal mesh parameters $h$ and $\tau$ satisfy $c\tau \le h \le C\tau$. Let $(\mathbb{V}_h, \mathbb{P}_h) \subset H_0^1(\Omega)^d \times L^2(\Omega)/\mathbb{R}$ be a div–stable pair of finite element spaces and $\mathbb{E}_h \subset L^2(\Omega)^{d\times d}$ be a classical finite element space. Assume that $\mathbb{V}_h$ and $\mathbb{E}_h$ contain the continuous piecewise quadratic functions and $\mathbb{P}_h$ the piecewise linear functions.*

*Let $\alpha$, $\beta \in \mathbb{R}$ and $We$, $\mu_s$, $\mu_p > 0$, and assume that $(v, p, E)$ is a smooth solution of equations (1.1) with strain energy given in equation (1.2). Let $\{(v_h, p_h, E_h)\}_{h>0}$ be solutions of the numerical scheme (3.4) with spaces $(\mathbb{V}_h, \mathbb{P}_h, \mathbb{E}_h)$, piecewise linear DG time stepping ($\ell = 1$), regularization of the determinant given in equation (3.8) with regularization parameter $c\tau \ln(1/\tau) \le \epsilon \le C\tau \ln(1/\tau)$, and initial data $(v_h^0, E_h^0)$ to be the spatial projections of $(v(0), E(0))$ characterized in Definition 4.1 for the space–time projection operator $\mathbb{P}_h^n$.*

*Then there exists constants $C > 0$ and $\tau_0$ independent of $h$, $\tau$ and $\epsilon$ such that the consistency error $(e_h, \mathcal{E}_h) = \mathbb{P}_h^n(v, E) - (v_h, E_h)$ satisfies*

$$\|e_h(t_{h-}^n)\|_{L^2(\Omega)}^2 + \frac{\mu_p}{We}\|\mathcal{E}_h(t_{h-}^n)\|_{L^2(\Omega)}^2 + \sum_{m=0}^{n-1}\left\{|\|[e_h^m]\|_{L^2(\Omega)}^2 + \frac{\mu_p}{We}|\|[\mathcal{E}_h^m]\|_{L^2(\Omega)}^2\right\}$$

$$\frac{\mu_p}{We}\int_0^{t_h^n}\int_{\mathcal{F}_h^0}|v_h \cdot n| \cdot [\mathcal{E}_h]^2 + \int_0^{t_h^n}\left\{\mu_s\|\nabla e_h\|_{L^2(\Omega)}^2 + \frac{\mu_p}{2We^2}\|\mathcal{E}_h\|_{L^2(\Omega)}^2\right\}$$

$$\le \left(\frac{1 + C\tau}{1 - C\tau}\right)^n\left\{\|e_h(0_-)\|_{L^2(\Omega)}^2 + \|\mathcal{E}_h(0_-)\|_{L^2(\Omega)}^2 + C\sum_{m=1}^n\left(d_h^m + \tau\epsilon^4\right)\right\}, \quad (4.2)$$

*for all $\tau < \tau_0$, where*

$$
\begin{aligned}
d_h^n = \int_{t_h^{n-1}}^{t_h^n} \Bigg\{ & ||p - p_{ph}||_{L^2(\Omega)}^2 + ||E||_{L^\infty[t^{n-1},t^n;L^\infty(\Omega)]}^2 ||\nabla e_p||_{L^2(\Omega)}^2 \\
& + \Big( ||v||_{L^\infty[t^{n-1},t^n;L^\infty(\Omega)]}^2 + ||\nabla v||_{L^\infty[t^{n-1},t^n;L^\infty(\Omega)]}^2 + ||\nabla E||_{L^\infty[t^{n-1},t^n;L^\infty(\Omega)]}^2 \Big) ||e_p||_{L^2(\Omega)}^2 \\
& + \Big( ||\nabla v||_{L^\infty[t^{n-1},t^n;L^\infty(\Omega)]}^2 + ||E||_{L^\infty[t^{n-1},t^n;L^\infty(\Omega)]}^2 \Big) ||\mathcal{E}_p||_{L^2(\Omega)}^2 \\
& + ||v_h||_{L^2(\Omega)}^2 \Big( ||\nabla e_p||_{L^\infty[t^{n-1},t^n;L^2(\Omega)]}^2 + ||e_p||_{L^\infty[t^{n-1},t^n;L^2(\Omega)]}^2 + ||\nabla \mathcal{E}_p||_{L^\infty[t^{n-1},t^n;L^2(\Omega)]}^2 \Big) \\
& + ||E_h||_{L^2(\Omega)}^2 \Big( ||\mathcal{E}_p||_{L^\infty[t^{n-1},t^n;L^2(\Omega)]}^2 + ||\nabla e_p||_{L^\infty[t^{n-1},t^n;L^2(\Omega)]}^2 \Big) \\
& + ||\nabla v_h||_{L^2(\Omega)}^2 ||\mathcal{E}_p||_{L^\infty[t^{n-1},t^n;L^2(\Omega)]}^2 + \frac{||(I - P_{\mathbb{E}_h})E||_{L^\infty[t^{n-1},t^n;L^\infty(\Omega)]}^2}{h^2} ||v_h||_{L^2(\Omega)}^2 \Bigg\},
\end{aligned}
$$

*and $(e_p, \mathcal{E}_p) = (I - \mathbb{P}_h^n)(v, E)$ is the projection error of the solution onto the discrete finite element spaces, and $p_{ph}$ is the projection of the pressure in $L^2[0,T;L^2(\Omega)]$ onto the finite element spaces.*

- For the meshes and spaces considered in this theorem

$$
\sum_{n=1}^{N_h} d_h^n \le C \left( ||v||_{W^{2,\infty}[0,T;W_0^{2,\infty}(\Omega)]^d}^2 + ||p||_{H^1[0,T;H^1(\Omega)]}^2 + ||E||_{W^{2,\infty}[0,T;W^{2,\infty}(\Omega)]^{d\times d}}^2 \right) (\tau^4 + h^4),
$$

  where $C$ only depends on $\Omega$.
- The hypotheses on the regularization parameter can be relaxed to: $\tau/\hat{c} \le \epsilon \le o(\tau^{d/4})$ for a sufficiently small constant $\hat{c}$ which depends upon the solution.

## 4.1. Overview of proof

This section presents the major steps required to prove Theorem 4.2 and the next two sections verify the estimates utilized. The latter are mostly routine application of Holder's inequality and estimates commonly used for the analysis of DG schemes. To improve the readability we write $t^n$ instead of $t_h^n$ below.

The theorem will be established by inducting on the time step $n$; the case $n = 0$ following directly from the assumptions on the initial data. The inductive step will follow upon selecting the test function in the orthogonality condition (4.1) to be the consistency error, $(w_h, G_h) = (e_h, \mathcal{E}_h)$. With this choice of test function coercivity of the bilinear form $a(.,.)$ and skew symmetry properties of $c(.,.,.)$ can be used to obtain

$$
\begin{aligned}
||e_h(t_-^n)||_{L^2(\Omega)}^2 & + \frac{\mu_p}{\text{We}} ||\mathcal{E}_h(t_-^n)||_{L^2(\Omega)}^2 + ||[e_h^{n-1}]||_{L^2(\Omega)} + \frac{\mu_p}{\text{We}} ||[\mathcal{E}_h^{n-1}]||_{L^2(\Omega)} \\
& + \frac{\mu_p}{\text{We}} \int_{t^{n-1}}^{t^n} \left\{ \sum_{F \in \mathcal{T}^{d-1}} \int_F |v_h \cdot n| \cdot [\mathcal{E}_h]^2 + \mu_s ||\nabla e_h||_{L^2(\Omega)}^2 + \frac{\mu_p}{2\text{We}^2} ||\mathcal{E}_h||_{L^2(\Omega)}^2 \right\} \\
& \le ||e_h(t_-^{n-1})||_{L^2(\Omega)}^2 + \frac{\mu_p}{\text{We}} ||\mathcal{E}_h(t_-^{n-1})||_{L^2(\Omega)}^2 + C d^n \\
& \quad + \int_{t^{n-1}}^{t^n} \left\{ C \left( ||e_h||_{L^2(\Omega)}^2 + ||\mathcal{E}_h||_{L^2(\Omega)}^2 \right) + 2(E^{-\top} - E_{h\epsilon}^{-\top}, \mathcal{E}_h) \right\}. \quad (4.3)
\end{aligned}
$$

If the last term was not present the result would follow from the discrete Gronwall inequality since the time dependence is piecewise linear;

$$
\int_{t^{n-1}}^{t^n} ||e_h||_{L^2(\Omega)}^2 \le \left( (1/2)||e_h(t_-^n)||_{L^2(\Omega)}^2 + ||e_h(t_-^{n-1})||_{L^2(\Omega)}^2 + ||[e_h^{n-1}]||_{L^2(\Omega)}^2 \right) \Delta t^n, \quad (4.4)
$$

and similarly for $\mathcal{E}_h$. In the first step of the proof we show that the determinant $\det(E_h)$ is bounded away from zero as $h \to 0$. We show that last term in equation (4.3) can be absorbed into the other terms to complete the inductive step.

(1) The regularization of the inverse determinant was chosen so that the map $E \mapsto E_\epsilon^{-\top}$ was a good approximation of $E^{-\top}$ when $\det(E)$ is positive and satisfied a global Lipschitz condition with constant $C/\epsilon$ in general. In this situation if $|E - E_p|$ is sufficiently small,

$$|E^{-\top} - E_{h\epsilon}^{-\top}| \leq |E^{-\top} - E_p^{-\top}| + |E_p^{-\top} - E_{p\epsilon}^{-\top}| + |E_{p\epsilon}^{-\top} - E_{h\epsilon}^{-\top}|$$
$$\leq C(\mathcal{E}_p + \epsilon^2) + (C/\epsilon)\mathcal{E}_h, \tag{4.5}$$

where $C = C(d, \delta, \Delta)$ with $\Delta = \|E\|_{L^\infty[0,T;L^\infty(\Omega)]}$, and $\delta > 0$ a lower bound on $\det(E)$. Substituting this bound into equation (4.3) gives an estimate for $\|\mathcal{E}_h\|_{L^2(\Omega)}$ of the form

$$\|\mathcal{E}_h(t_-^n)\|_{L^2(\Omega)}^2 + \|[\mathcal{E}_h^{n-1}]\|_{L^2(\Omega)}^2 \leq C \left( \frac{1 + (C/\epsilon)\Delta t^n}{1 - (C/\epsilon)\Delta t^n} \right) \left( \|e_h(t_-^{n-1})\|_{L^2(\Omega)}^2 + \|\mathcal{E}_h(t_-^{n-1})\|_{L^2(\Omega)}^2 + d^n + \epsilon^2 \right).$$

By hypothesis[2] $\Delta t^n/\epsilon \leq C/\ln(1/\tau) \to 0$ in which case the inductive assumption shows

$$\|\mathcal{E}_h(t_-^n)\|_{L^2(\Omega)}^2 + \|[\mathcal{E}_h^{n-1}]\|_{L^2(\Omega)}^2 \leq C(h^2 + \tau^2 + \epsilon^2)^2,$$

with constant independent of $(h, \tau, \epsilon)$ for $\tau$ sufficiently small. The inverse inequality for functions in $\mathbb{E}_h$, and the assumption $c \leq h/\tau \leq C$, then provides an $L^\infty(\Omega)$ bound,

$$\|\mathcal{E}_h(t_-^n)\|_{L^\infty(\Omega)} + \|[\mathcal{E}_h^{n-1}]\|_{L^\infty(\Omega)} \leq C \left( h^2 + \tau^2(1 + \ln^2(1/\tau)) \right)/h^{d/2} \leq C \ln^2(1/\tau)\tau^{2-d/2}.$$

Since $d \leq 3$ the $L^\infty(\Omega)$ norm of the consistency error becomes arbitrarily small as $\tau \to 0$ and the triangle inequality then guarantees $E_h$ becomes uniformly close to $E$;

$$\|E - E_h\|_{L^\infty[t^{n-1},t^n;L^\infty(\Omega)]} \leq \|\mathcal{E}_p\|_{L^\infty[t^{n-1},t^n;L^\infty(\Omega)]} + \|\mathcal{E}_h\|_{L^\infty[t^{n-1},t^n;L^\infty(\Omega)]} \leq C \ln^2(1/\tau)\tau^{2-d/2}.$$

In particular, since $E \mapsto \det(E)$ is continuous and $\det(E(t,x)) \geq \delta > 0$ it follows that

$$\det(E_h(t,x)) \geq \delta/2 \qquad (t,x) \in (t^{n-1}, t^n) \times \Omega,$$

when $\tau$ is sufficiently small.

(2) The regularization of the inverse determinant was chosen so that the map $E \mapsto E_\epsilon^{-\top}$ is Lipschitz with constant independent of $\epsilon$ on bounded sets with $\det(E)$ bounded away from zero. In this situation equation (4.5) becomes

$$|E^{-\top} - E_{h\epsilon}^{-\top}| \leq C(\mathcal{E}_p + \epsilon^2 + \mathcal{E}_h). \tag{4.6}$$

Substituting this bound into equation (4.3) shows

$$\|e_h(t_-^n)\|_{L^2(\Omega)}^2 + \frac{\mu_p}{\text{We}}\|\mathcal{E}_h(t_-^n)\|_{L^2(\Omega)}^2 + \|[e_h^{n-1}]\|_{L^2(\Omega)} + \frac{\mu_p}{\text{We}}\|[\mathcal{E}_h^{n-1}]\|_{L^2(\Omega)}$$
$$+ \frac{\mu_p}{\text{We}} \int_{t^{n-1}}^{t^n} \left\{ \sum_{F \in \mathcal{T}^{d-1}} \int_F |v_h \cdot n| \cdot [\mathcal{E}_h]^2 + \mu_s\|\nabla e_h\|_{L^2(\Omega)}^2 + \frac{\mu_p}{2\text{We}^2}\|\mathcal{E}_h\|_{L^2(\Omega)}^2 \right\}$$
$$\leq \|e_h(t_-^{n-1})\|_{L^2(\Omega)}^2 + \frac{\mu_p}{\text{We}}\|\mathcal{E}_h(t_-^{n-1})\|_{L^2(\Omega)}^2 + Cd^n$$
$$+ C \int_{t^{n-1}}^{t^n} \left\{ \|e_h\|_{L^2(\Omega)}^2 + \|\mathcal{E}_h\|_{L^2(\Omega)}^2 + \epsilon^2 \right\}.$$

---

[2]The hypothesis $c \leq \epsilon/(\tau \ln(1/\tau))$ is used to guarantee $1 - C\epsilon/\tau$ is eventually bounded away from zero; clearly "$\epsilon/\tau$ sufficiently small" suffices.

Using equation (4.4) to bound the integrals on the last line and the inductive hypothesis to bound the first two terms on the right completes the induction step.

In the next section the estimates needed to verify equation (4.3) are developed, and the following section shows that the regularization of the inverse transpose given in (3.8) satisfies the Lipschitz conditions stated in equations (4.5) and (4.6).

### 4.2. Coercivity of the weak statement

In this section the estimates which establish the coercivity properties stated in equation (4.3) are developed.

**Bilinear terms.** Bounds on the bilinear terms in the weak statement are standard.

(1) *Temporal terms*: The projection in Definition 4.1 is frequently used to analyze DG time stepping methods [30]. When the exact solution is continuous in time the temporal terms in the orthogonality condition become

$$\int_{t^{n-1}}^{t^n} (v_t - v_{ht}, e_h) + ([v^{n-1}], e_h^{n-1}) = \frac{1}{2} \left( \|e_{h-}^n\|_{L^2(\Omega)}^2 + \|[e_h^{n-1}]\|_{L^2(\Omega)}^2 - \|e_{h-}^{n-1}\|_{L^2(\Omega)}^2 \right),$$

and similarly for the deformation $E - E_h$.

(2) *Spatial terms*: The coercivity of the bilinear terms is standard;

$$a((v - v_h, E - E_h), (e_h, \mathcal{E}_h)) = a((e_h, \mathcal{E}_h), (e_h, \mathcal{E}_h)) + a((e_p, \mathcal{E}_p), (e_h, \mathcal{E}_h))$$

$$\geq \left( \mu_s \|D(e_h)\|_{L^2(\Omega)}^2 + \frac{\mu_p}{4\mathrm{We}^2} \|\mathcal{E}_h\|_{L^2(\Omega)}^2 \right) - \left( \mu_s \|D(e_p)\|_{L^2(\Omega)}^2 + \frac{\mu_p}{4\mathrm{We}^2} \|\mathcal{E}_p\|_{L^2(\Omega)}^2 \right),$$

and since $e_h$ takes values in $\mathbb{Z}_h$

$$(p - p_h, \mathrm{div}(e_h)) = (p, \mathrm{div}(e_h)) = (p - q_h, \mathrm{div}(e_h)), \qquad q_h \in \mathbb{P}_h.$$

**Trilinear and jump terms.** The skew symmetry properties of the trilinear term are used to eliminate the term cubic in $(e_h, \mathcal{E}_h)$. The first step is to write

$$c((v, E), (v, E), (e_h, \mathcal{E}_h)) - c((v_h, E_h), (v_h, E_h), (e_h, \mathcal{E}_h))$$
$$= c((e_p, \mathcal{E}_p), (v, E), (e_h, \mathcal{E}_h)) + c((v_h, E_h), (e_p, \mathcal{E}_p), (e_h, \mathcal{E}_h))$$
$$+ c((e_h, \mathcal{E}_h), (v, E), (e_h, \mathcal{E}_h)) + c((v_h, E_h), (e_h, \mathcal{E}_h), (e_h, \mathcal{E}_h)). \quad (4.7)$$

The trilinear term was constructed so that the only deformation to be differentiated is the one in the second argument, $c((.,.), (., F), (.,.))$. In this situation Holder's inequality can be used to bound the first three terms in the above as

$$c((e_p, \mathcal{E}_p), (v, E), (e_h, \mathcal{E}_h)) + c((v_h, E_h), (e_p, \mathcal{E}_p), (e_h, \mathcal{E}_h)) + c((e_h, \mathcal{E}_h), (v, E), (e_h, \mathcal{E}_h))$$
$$\leq C d_h^n + \int_{t^{n-1}}^{t^n} \left\{ (\mu_s/2) \|D(e_h)\|_{L^2(\Omega)}^2 + C \left( \|e_h\|_{L^2(\Omega)}^2 + \|\mathcal{E}_h\|_{L^2(\Omega)}^2 \right) \right\}.$$

When developing this expression Korn's inequality is used to bound $\nabla e_h$ by its symmetric part and the constants are managed so that the term involving $D(e_h)$ can be absorbed by $a((e_h, .), (e_h, .))$.

To bound the final term in equation (4.7) note that $c(., ., .)$ is almost skew symmetric in the last argument,

$$c((v_h, E_h), (e_h, \mathcal{E}_h), (e_h, \mathcal{E}_h)) = \sum_K \int_{t^{n-1}}^{t^n} \int_K ((v_h.\nabla)\mathcal{E}_h, \mathcal{E}_h) + (1/2)\mathrm{div}(v_h)\|\mathcal{E}_h\|_{L^2(\Omega)}^2$$

$$= \frac{1}{2} \sum_{K \subset \mathcal{T}} \int_{t^{n-1}}^{t^n} \int_K (v_h.n) |\mathcal{E}_{h-}|^2,$$

and the DG scheme is engineered to stabilize the jump terms. Specifically,

$$
\begin{aligned}
c((v_h, E_h), &(e_h, \mathcal{E}_h), (e_h, \mathcal{E}_h)) + J_h(v_h, E_h, \mathcal{E}_h) \\
&= c((v_h, E_h), (e_h, \mathcal{E}_h), (e_h, \mathcal{E}_h)) - J_h(v_h, \mathcal{E}_h, \mathcal{E}_h) + J_h(v_h, E_p, \mathcal{E}_h) \\
&= \frac{1}{2} \sum_{F \subset \mathcal{T}^{d-1}} \int_{t^{n-1}}^{t^n} \int_F |v_h.n|\, |[\mathcal{E}_h]|^2 + J_h(v_h, E_p, \mathcal{E}_h).
\end{aligned}
$$

To bound the final term, recall that the dependence of $J_h(.,.,.)$ upon its second argument is through its jump, and since $\mathbb{P}^n(E)$ is (spatially) continuous

$$
J_h(v_h, E_p, \mathcal{E}_h) = J_h(v_h, E_p - \mathbb{P}^n(E), \mathcal{E}_h) = J_h(v_h, \mathbb{P}^n(P_{\mathbb{E}_h}(E) - E), \mathcal{E}_h).
$$

Using the finite dimensionality of $\mathbb{V}_h$ and $\mathbb{E}_h$ a parent element argument shows

$$
\int_{t^{n-1}}^{t^n} J_h(v_h, \mathcal{E}_p, \mathcal{E}_h) \leq C \int_{t^{n-1}}^{t^n} \|v_h\|_{L^2(\Omega)} \|\mathcal{E}_h\|_{L^2(\Omega)} \max_K \frac{\|(I - P_{\mathbb{E}_h})E\|_{L^\infty(K)}}{h_K} \leq C \int_{t^{n-1}}^{t^n} \|\mathcal{E}_h\|_{L^2(\Omega)}^2 + C d_h^n.
$$

### 4.3. Lipschitz continuity of the regularization

This section is devoted to the proof of the estimates (4.5) and (4.6). The following lemma is a convenient statement of the property that matrix inversion is locally Lipschitz on the set of non–singular matrices.

**Lemma 4.3.** *Let $E, E_p \in \mathbb{R}^{d \times d}$ and suppose that $\det(E) > \delta$. Then there exist $c = c(d, \delta, |E|) > 0$ and $C = C(d, \delta, |E|) > 0$ such that*

$$
|E - E_p| \leq c \qquad \Rightarrow \qquad |E^{-T} - E_p^{-T}| \leq C|E - E_p|.
$$

The next lemma establishes the continuity properties of the regularized inverse transpose; the estimates asserted in equations (4.5) and (4.6) follow directly from these.

**Lemma 4.4.** *Let $E_\epsilon^{-\top} = (1/\det_\epsilon(E))\mathrm{Cof}(E)$ where $\det_\epsilon(E)$ is the regularization of the determinant given in equation (3.8), and write*

$$
M(\delta, \Delta) = \{E \in \mathbb{R}^{d \times d} \mid \delta \leq \det(E) \text{ and } |E| \leq \Delta\}.
$$

*Then for each $\delta, \Delta > 0$ there exists a constant $C = C(d, \delta, \Delta) > 0$ independent of $0 < \epsilon \leq 1$ such that the following holds.*

(1) $|E^{-\top} - E_\epsilon^{-\top}| = O(\epsilon^2)$ *on $M(\delta, \Delta)$; that is,*

$$
E \in M(\delta, \Delta) \qquad \Rightarrow \qquad |E^{-\top} - E_\epsilon^{-\top}| \leq C\epsilon^2.
$$

(2) *The mapping $E \mapsto E_\epsilon^{-\top}$ is locally Lipschitz on the set of matrices with positive determinant; in particular,*

$$
E, F \in M(\delta, \Delta) \qquad \Rightarrow \qquad |E_\epsilon^{-\top} - F_\epsilon^{-\top}| \leq C|E - F|.
$$

(3) *The mapping $E \mapsto E_\epsilon^{-\top}$ satisfies the global Lipschitz property*

$$
E \in M(\delta, \Delta) \qquad \Rightarrow \qquad |E_\epsilon^{-\top} - F_\epsilon^{-\top}| \leq (C/\epsilon)|E - F|, \quad F \in \mathbb{R}^{d \times d}.
$$

*Proof.*

(1) Fix $E \in M(\delta, \Delta)$ and compute

$$
\begin{aligned}
E^{-\top} - E_\epsilon^{-\top} &= \left( \frac{1}{\det E} - \frac{1}{\det_\epsilon(E)} \right) \mathrm{Cof}(E) \\
&= \frac{\sqrt{\det(E)^2 + 4\epsilon^2 + \epsilon^2 |E|^{2(d-1)}} - \det(E)}{\sqrt{\det(E)^2 + 4\epsilon^2 + \epsilon^2 |E|^{2(d-1)}} + \det(E)} \, \mathrm{Cof}(E) \\
&= \frac{\left( 4 + |E|^{2(d-1)} \right) \epsilon^2}{\left( \sqrt{\det(E)^2 + 4\epsilon^2 + \epsilon^2 |E|^{2(d-1)}} + \det(E) \right)^2} \, \mathrm{Cof}(E)
\end{aligned}
$$

The right hand side is of order $O(\epsilon^2)$ uniformly for matrices $E \in M(\delta, \Delta)$.

(2) The mappings $E \mapsto \mathrm{Cof}(E)$ and $E \mapsto \det_\epsilon(E)$ are smooth so their derivatives are locally bounded. Since $M(\delta, \Delta)$ is compact and $\det_\epsilon(E) \geq \delta$ on this set, Lipschitz continuity of $(1/\det_\epsilon(E))\mathrm{Cof}(E)$ follows.

(3) Let $E \in M(\delta, \Delta)$ and $F \in \mathbb{R}^{d \times d}$. If $F \in M(\delta/2, 2\Delta)$ then so too is $E$ and this reduces to the case considered in (2) above, so it suffices to consider $F \notin M(\delta/2, 2\Delta)$. Below we show

$$
E \in M(\delta, \Delta) \text{ and } F \notin M(\delta/2, 2\Delta) \qquad \Rightarrow \qquad |E - F| \geq 1/C.
$$

Granted this the Lipschitz estimate follows;

$$
|E_\epsilon^{-\top} - F_\epsilon^{-\top}| \leq |E_\epsilon^{-\top}| + |F_\epsilon^{-\top}| \leq (C/\epsilon) \leq (C/\epsilon) C |E - F|.
$$

To show $|E - F| \geq 1/C$ we consider the two possibilities which preclude $F$ from $M(\delta/2, 2\Delta)$.

(1) If $|F| > 2\Delta$ it is immediate that $|E - F| \geq \Delta$ when $|E| \leq \Delta$.

(2) If $|F| \leq 2\Delta$ it must be that $\det(F) < \delta/2$. Since $\det(E) \geq \delta$,

$$
\delta/2 \leq |\det(E) - \det(F)| \leq C |E - F|,
$$

where $C$ is the Lipschitz constant for the mapping $E \mapsto \det(E)$ on the (compact) set of matrices with norm bounded by $2\Delta$. $\qquad \square$

## 5. EXTENSIONS

The assumption that $v$ satisfied homogeneous boundary data circumvents a multitude of technical and modeling issues. Since most flow problems involve inflow and outflow boundaries where velocity or stress components are specified this is a significant practical limitation. Note too that boundary data for the deformation needs to be specified on the portion of the boundary where $v.n < 0$ and the latter may depend implicitly upon time. One way to accommodate these issues is to include a penalty term with parameter $\eta > 0$ to enforce non–zero boundary data. Specifically, if $\partial\Omega = \bar{\Gamma}_0 \cup \bar{\Gamma}_1$ and Dirichlet data for the velocity, $v|_{\Gamma_0} = v_0$, is specified on $\Gamma_0$, and traction boundary data, $g$, is specified on $\Gamma_1$, a practical modification of (3.5) is

$$
\begin{aligned}
&\int_{t^{n-1}}^{t^n} \left\{ (v_{ht}, w_h) + \frac{\mu_p}{\mathrm{We}} (E_{ht}, G_h) + a((v_h, E_h), (w_h, G_h)) - (p_h, \mathrm{div}(w_h)) + (q_h, \mathrm{div}(v_h)) \right. \\
&\qquad \left. + c((v_h, E_h), (v_h, E_h), (w_h, G_h)) + J_h(v_h, E_h, G_h) - \frac{\mu_p}{2\mathrm{We}^2} (E_{h\epsilon}^{-T}, G_h) \right\} \\
&\quad + \int_{t^{n-1}}^{t^n} \left\{ \int_{\Gamma_0} \frac{1}{\eta}(v_h - v_0, w_h) + \int_{\partial\Omega} (v.n)^- (E_h - E_0, G_h) \right\} \\
&\quad + \left( [v_h]^{n-1}, w_h(t_+^{n-1}) \right) + \frac{\mu_p}{\mathrm{We}} \left( [E_h]^{n-1}, G_h(t_+^{n-1}) \right) = \int_{t^{n-1}}^{t^n} \left\{ (f, w_h) + \int_{\Gamma_1} (g, w_h) \right\}, \qquad (5.1)
\end{aligned}
$$

where $E_0$ is boundary data for the deformation. Solutions of this weak statement satisfy

$$\|v_{h-}^n\|_{L^2(\Omega)}^2 + \frac{\mu_p}{\mathrm{We}}\|E_{h-}^n\|_{L^2(\Omega)}^2 + \sum_{m=0}^{n-1}\left(\|[v_h^m]\|_{L^2(\Omega)}^2 + \frac{\mu_p}{\mathrm{We}}\|[E_h^m]\|_{L^2(\Omega)}\right)$$

$$+ \int_0^{t^n}\left\{2\mu_s\|D(v_h)\|_{L^2(\Omega)}^2 + \frac{\mu_p}{\mathrm{We}^2}\|E_h\|_{L^2(\Omega)}^2 + 2d\|\det(E_h)^-/\det_\epsilon(E_h)\|_{L^1(\Omega)}\right\}$$

$$+ \int_0^{t^n}\left\{\frac{1}{\eta}\left(\|v_h\|_{L^2(\Gamma_0)}^2 + \|\bar{v}_h - v_0\|_{L^2(\Gamma_0)}^2\right) + \int_{\partial\Omega}(v_h.n)^-\left(|E_h|^2 + |E_h - E_0|^2\right)\right\}$$

$$+ \frac{\mu_p}{\mathrm{We}}\sum_{F\in\mathcal{T}_h^{d-1}}\int_0^{t^n}\int_F |v_h\cdot n|\,[E_h]^2 \leq \|v_{h-}^0\|_{L^2(\Omega)}^2 + \frac{\mu_p}{\mathrm{We}}\|E_{h-}^0\|_{L^2(\Omega)}^2 + \frac{\mu_p}{\mathrm{We}^2}d|\Omega|t^n$$

$$+ \int_0^{t^n}\left\{\frac{1}{\mu_s}\|f\|_{H^{-1}(\Omega)}^2 + C\|g\|_{H^{-1/2}(\Gamma_1)}^2 + \frac{1}{\eta}\|v_0\|_{L^2(\Gamma_0)}^2 + \int_{\partial\Omega}(v_h.n)^-|E_0|^2\right\}.$$

The boundary terms in (5.1) were constructed so that the stability estimate and existence would follow. With this choice the natural boundary condition for the momentum equation becomes

$$\left((\rho/2)v\otimes v - pI + 2\mu_s D(v) + \frac{\mu_p}{\mathrm{We}}(a+b)(EE^\top - I)\right)n = g.$$

If a vortex exits the domain the sign of $v.n$ may change on $\Gamma_1$. This gives rise to a modeling problem: what is the value of $E$ on the reentrant boundary?

## 5.1. Higher order approximation

It was shown in Section 3 that numerical solutions $(v_h, E_h)$ are bounded in $L^2[0, T; H^1(\Omega)] \times L^2[0, T; L^2(\Omega)]$ and that $(v_h(t_{h\pm}^n), E_h(t_{h\pm}^n))$ is bounded in $L^2(\Omega) \times L^2(\Omega)$ at the partition points. When low order $(\ell \leq 1)$ polynomial approximation is used for the time variable a bound at the partition points bounds the solution in $L^\infty[0, T; L^2(\Omega)]$; this was required for the convergence proof in Section 4. If a higher order polynomial approximation is used for the time variable, then bounds in $L^\infty[0, T; L^2(\Omega)]$ are no longer immediate. However, uniform bounds on the solutions are available if Radau quadrature is used to approximate the temporal integrals of the nonlinear terms, $c(.,.,.)$, $J_h(.,.,.)$ and $E_{h\epsilon}^{-\top}$, in the discrete weak statement (3.5).

If $t^{n-1} = s_0 < s_1 < \ldots < s_\ell < t^n$ are the (left handed) Radau points in $[t^{n-1}, t^n)$ and $\{\omega_i\}_{i=0}^\ell \subset (0, 1)$ the corresponding weights, then the quadrature rule

$$Q(f) = (t^n - t^{n-1})\sum_{i=0}^\ell \omega_i f(s_i),$$

is exact on $\mathcal{P}_{2\ell}(t^{n-1}, t^n)$, so all of the bilinear terms in (3.5) are integrated exactly by this quadrature rule. To obtain uniform bounds upon the solution let $\{\phi_i\}_{i=0}^\ell \subset \mathcal{P}_\ell(t^{n-1}, t^n)$ denote the Lagrange basis corresponding to the quadrature points $(\phi_i(s_j) = \delta_{ij})$ and write

$$v_h(t) = \sum_{i=0}^\ell v_i\phi_i(t), \qquad v_i \in \mathbb{V}_h,$$

and similarly for $E_h$. Set $\theta(t) = 1 - (t - t^{n-1})/(t^n - t^{n-1}) \in [0, 1]$ and select the test function $w_h$ to be

$$w_h(t) = \sum_{i=0}^\ell \theta(s_i)v_i\phi_i(t),$$

and similarly for $G_h$. Uniform bounds then follow from the following properties.

- $(v_{ht}(s_i), w_h(s_i)) = \theta(s_i)(v_{ht}(s_i), v_h(s_i))$ is the interpolant of $\theta(v_{ht}, v_h) \in \mathcal{P}_{2\ell}(t^{n-1}, t^n)$ so

$$\int_{t^{n-1}}^{t^n} (v_{ht}, w_h) + ([v_h], w_{h+})^{n-1} = \int_{t^{n-1}}^{t^n} \theta(v_{ht}, v_h) + ([v_h], w_{h+})^{n-1}$$

$$= \frac{1/2}{t^n - t^{n-1}} \int_{t^{n-1}}^{t^n} \|v_h\|_{L^2(\Omega)}^2 + (1/2)\|[v_h^{n-1}]\|_{L^2(\Omega)}^2 - (1/2)\|v_{h-}^{n-1}\|_{L^2(\Omega)}^2,$$

and similarly for $E_h$. Left handed Radau quadrature was chosen so that the jump terms take the form shown. The key step is to use the inverse estimate for the polynomial $\|v_h(t)\|_{L^2(\Omega)}^2 \in \mathcal{P}_{2\ell}(t^{n-1}, t^n)$ to conclude

$$\|v_h\|_{L^\infty[t^{n-1}, t^n; L^2(\Omega)]}^2 \leq \frac{C}{t^n - t^{n-1}} \int_{t^{n-1}}^{t^n} \|v_h\|_{L^2(\Omega)}^2.$$

- Since the weak statement is linear in the test functions the constants $\theta(s_i)$ can be factored out of the spatial operators so that the skew symmetry and monotonicity are preserved; for example,

$$c((u, E), (v, F), (v, \theta F)) + J_h(u, F, \theta F) = \frac{\mu_p}{2\mathrm{We}} \sum_{F \in \mathcal{T}_h^{d-1}} \theta \int_F |u.n| \, |[F]|^2.$$

The convergence proof in Section 4 then extends to schemes of arbitrary order in space and time. However, due the the assumption $\epsilon = O(\tau \ln(1/\tau))$, more accurate regularizations of the determinant will be required to achieve higher rates.

## 5.2. Other fluids

The analysis in Sections 3 and 4 focused on the Oldroyd–B fluids; however, the extension to many of the classical viscoelastic fluids is direct provided the solvent viscosity $\mu_s$ is non–zero. The deformation of the Oldroyd–B fluid evolves according to the "maximum dissipation principle" which postulates a gradient flow of the elastic energy. Different models of viscoelastic relaxation give rise to equations of the form

$$\dot{E} - \alpha(\nabla v)E - \beta(\nabla v)^\top E + \mathcal{D}(E) = 0,$$

where $\mathcal{D}(E) : D\mathcal{W}(E) \geq 0$ characterizes the dissipation as the stress relaxes.

- *Phan–Thien–Tanner (PPT) Fluid:* $\mathcal{D}(E) = (\mu_p/\mathrm{We})(|E|^2 E - E^{-\top}) = D\mathcal{R}(E)$ where the "Raleighian" is

$$\mathcal{R}(E) = \frac{\mu_p}{\mathrm{We}} \left((1/4)(|E|^4 - |I|^4) - (1/2)\ln(\det(E)^2)\right).$$

- *Giesekus Fluid:* $\mathcal{D}(E) = (\mu_p/\mathrm{We})(EE^\top E - E^{-\top}) = D\mathcal{R}(E)$ with Raleighian

$$\mathcal{R}(E) = \frac{\mu_p}{\mathrm{We}} \left((1/4)(|EE^\top|^2 - |I|^2) - (1/2)\ln(\det(E)^2)\right).$$

The extension of the analysis presented for the Oldroyd–B to these fluids is direct.

Other fluid models retain the maximal dissipation principle but modify the elastic energy $\mathcal{W}$. Typically

$$\mathcal{W}(E) = \frac{\mu_p}{2\mathrm{We}} \left(\psi\left(|E|^2\right) - \psi'\left(|I|^2\right) \log\left(\det(E)^2\right)\right),$$

where $\psi : (0, \infty) \to \mathbb{R}$ is a monotone increasing convex function. Then

$$D\mathcal{W}(E) = \frac{\mu_p}{\mathrm{We}} \left(\psi'\left(|E|^2\right)E - \psi'\left(|I|^2\right)E^{-\top}\right),$$

is frame indifferent and vanishes at the identity.

- *Finitely Extensible Nonlinear Elastic (FENE–P) Fluid:* $\mathcal{W}(E) \sim \ln(1 - |E|^2/|E_0|^2)$ where $|E_0| > |I|$ is an upper bound on the deformation the polymer can sustain.

$$\mathcal{W}(E) = -\frac{\mu_p}{2\mathrm{We}} \left( \ln \left( \frac{|E_0|^2 - |E|^2}{|E_0|^2 - |I|^2} \right) + \frac{\ln(\det(E)^2)}{|E_0|^2 - |I|^2} \right)$$

with Piola stress

$$D\mathcal{W}(E) = \frac{\mu_p}{\mathrm{We}} \left( \frac{E}{|E_0|^2 - |E|^2} - \frac{E^{-\top}}{|E_0|^2 - |I|^2} \right).$$

The Yosida approximation [32] provides a regularization of the first term with globally Lipschitz derivative. This can be calculated using the Yosida approximation of $\phi(u) = -\ln(1 - u^2)$;

$$\phi_\epsilon(u) = \frac{1}{2\epsilon}(u_\epsilon - u)^2 + \phi(u_\epsilon),$$

where $u_\epsilon$ is the root of $x^3 - ux^2 - (1 + \epsilon)x + u$ in $(-1, 1)$,

$$u_\epsilon = \frac{2}{3}\sqrt{3 + 3\epsilon + u^2} \cos\left( \frac{\pi}{3} + \frac{1}{3}\arccos\left( \frac{u\left(-2u^2 + 18 - 9\epsilon\right)}{2\left(3 + 3\epsilon + u^2\right)^{3/2}} \right) \right) + \frac{u}{3}.$$

Stable numerical schemes for these fluids can be developed from the weighted weak statement

$$\int_\Omega \left( \dot{E} - \alpha(\nabla v)E - \beta(\nabla v)^\top E + D\mathcal{W}(E), \psi'(|E|^2)G \right) = 0,$$

provided the jump terms for the DG scheme also include the weight;

$$\int_{t^{n-1}}^{t^n} \left\{ \int_\Omega (\dot{E} - \alpha(\nabla v_h)E_h - \beta(\nabla v_h)^\top E_h, G_h) + \frac{1}{2}\mathrm{div}(v_h)(E_h, G_h) + D\mathcal{W}(E_h), \psi'(|E_h|^2)G_h) \right.$$

$$\left. + \sum_{K \in \mathcal{T}_h} \int_{\partial K} (v_h \cdot n)^- ([E_h], \psi'(|E_{h-}|^2)G_{h-}) \right\} + \int_\Omega ([E_h^{n-1}], \psi'(|E_{h+}^{n-1}|^2)G_h(t_+^{n-1})) = 0.$$

The jump terms in the energy estimate take the form

$$\left( \psi'(|E_+|^2)E_+ - \psi'(|E_-|^2)E_-, E_+ - E_- \right) \geq 0.$$

Weighted DG schemes to simulate gradient flows with (non-quadratic) convex energies have not be implemented to date.

## 6. NUMERICAL EXAMPLES

To illustrate the results developed in Sections 3 and 4 numerical approximation of a channel flow for which an exact solution is available is presented. We then present some preliminary computations for two benchmark problems in two dimensions; a 4:1 contraction and flow past a disk. While quantitative data for the later two problems computed using alternative schemes is available, a precise comparison is complicated since it is not clear that solution of problems driven by non–homogeneous boundary data are stationary; or alternatively, stationary solutions may not be stable [1].

In all of the examples the nonlinear algebraic equations were solved using Newton's method with a direct linear solver and halting tolerance (change in any variable) $10^{-8}$. If the Newton scheme for a particular time step failed it was subdivided into two steps recursively until convergence was attained. The Yosida approximation (3.7) was used to regularize the inverse of the determinant of the deformation.

| $\tau$ | $\mathbb{V}_h \times \mathbb{P}_h \times \mathbb{E}_h = Q'_2 \times Q_1 \times Q_1$, $h = 2\tau$ and $\ell = 1$ | | |
|---|---|---|---|
| | $|v - v_h|_{L^2[0,T;H^1(\Omega)]}$ | $\|p - p_h\|_{L^2[0,T;L^2(\Omega)]}$ | $\|E - E_h\|_{L^2[0,T;L^2(\Omega)]}$ |
| 1/8 | 1.663865e-02 | 5.652340e-02 | 4.465875e-02 |
| 1/16 | 4.647908e-03 | 2.668692e-02 | 1.144977e-02 |
| 1/32 | 1.255666e-03 | 1.306950e-02 | 2.883085e-03 |
| 1/64 | 3.325136e-04 | 6.471380e-03 | 7.225167e-04 |
| Norms | 2.110391 | 2.063824 | 3.125278 |

FIGURE 2. Channel flow: Linear elements for deformation, $\epsilon = \tau/10$, We $= 1.25$.

Results for the two benchmark problems are typically presented for inertialess (creeping or Stokes) flows, so for these problems we set $\rho = 0$. For these problems the regularization parameter was fixed at $\epsilon = 10^{-6}$. In order to minimize transient elastic waves the initial data was taken to be $(v^0, E^0) = (0, I)$ and non–homogeneous boundary data for the velocity was ramped up to the desired magnitude with a trigonometric profile, $(1/2)(1 - \cos(\pi t))v_0(x)$ for $0 \leq t \leq 1$. The deformation on the inflow (left hand) boundary was specified to be the identity matrix.

## 6.1. Channel flow

An exact solution for parallel flow of an Oldroyd–B fluid in a channel, $\Omega = (-1,1)^2$, with $\rho = 1$, $p = (p_0 + p_1 x)e^{t/\lambda}$, and $f = 0$, is

$$v(t,y) = p_1 \lambda e^{t/\lambda} \begin{pmatrix} \frac{\cosh(ay) - \cosh(a)}{\cosh(a)} \\ 0 \end{pmatrix} \quad \text{where} \quad a = \sqrt{\frac{\text{We} + \lambda}{\lambda(\text{We}\mu + \lambda\mu + \lambda\mu_p)}}$$

and $T_e = (\mu_p/\text{We})(VV^\top - I)$ where

$$V = \begin{bmatrix} \sqrt{1+b} & v_{12} \\ 0 & 1 \end{bmatrix} \quad \text{with} \quad v_{12} = \frac{\text{We}}{\text{We} + \lambda} \frac{a \sinh(ay)}{\cosh(a)} p_1 \lambda^2 e^{t/\lambda} \quad \text{and} \quad b = \frac{\lambda}{2\text{We} + \lambda} v_{12}^2.$$

The general solution of the corresponding deformation equation is $E = VR$ with

$$R = \begin{bmatrix} \cos(\theta) & \sin(\theta) \\ -\sin(\theta) & \cos(\theta) \end{bmatrix} \quad \text{with} \quad \theta = \frac{\lambda}{2\text{We}} \frac{\log(\sqrt{1+b} + \sqrt{b})}{\sqrt{b}} v_{12} + \Theta(x - \lambda v_1),$$

where $\Theta : \mathbb{R} \to \mathbb{R}$ is arbitrary. In the following computations $p_0 = 0$, the pressure gradient is $p_1 = -1$, the time constant is $\lambda = 1$, and the non–zero choice $\Theta(\xi) = \sin(\xi)$ is made to give a deformation $E(t,x,y)$ depending upon all of the variables. In the numerical experiments the velocity is specified at the inlet $x = -1$ and the channel walls $y = \pm 1$; the traction is specified at the outlet $x = 1$; and the deformation is specified on the inflow boundary $x = -1$.

No evidence of a HWNP was encountered computing numerical approximations of this problem. The following three tests illustrate the properties of the algorithm and numerical solutions. In each of the tests the viscosities were $\mu_s = 0.25$, $\mu_p = 0.75$, and a finial time of $T = 1$ and uniform square grids were utilized.

- *Rate of Convergence*: The proof of Theorem 4.2 required the deformation to be approximated by quadratic elements in order to attain a second order rate; however, formally the scheme is second order when linear elements are used for this variable. Errors in the solutions computed using bilinear ($Q_1$) and serendipity biquadratic ($Q'_2$) elements for the deformation and the classical Taylor Hood pair $Q'_2 \times Q_1$ for the velocity and pressure are presented in Figures 2 and 3. The quadratic rate of convergence for the velocity and deformation is readily observable in each case. Unlike solutions of the Navier Stokes equations, the pressure only converges at a first order rate; the reason for this requires further investigation. In all instances the Newton scheme converged in three or four iterates.

| $\tau$ | $\mathbb{V}_h \times \mathbb{P}_h \times \mathbb{E}_h = Q_2' \times Q_1 \times Q_2'$, $h = 2\tau$ and $\ell = 1$ | | |
|---|---|---|---|
| | $|v - v_h|_{L^2[0,T;H^1(\Omega)]}$ | $\|p - p_h\|_{L^2[0,T;L^2(\Omega)]}$ | $\|E - E_h\|_{L^2[0,T;L^2(\Omega)]}$ |
| 1/8 | 9.158628e-03 | 5.298274e-02 | 5.630538e-03 |
| 1/16 | 2.333355e-03 | 2.623177e-02 | 1.240301e-03 |
| 1/32 | 5.936999e-04 | 1.301273e-02 | 2.968640e-04 |
| 1/64 | 1.518414e-04 | 6.464310e-03 | 7.329059e-05 |

FIGURE 3. Channel flow: Quadratic elements for deformation, $\epsilon = 0.1\tau$, We $= 1.25$.

- *Weissenberg number:* For this example, the Weissenberg number had minimal influence on the numerical performance of the algorithm. For example, with the parameters as in Figure 3 and $h = 1/16$ the code required an identical number of Newton iterations for We $\in \{0.125, 1.25, 12.5, 125\}$. Norms of the deformation for these Weissenberg numbers are:

| We | 0.125 | 1.25 | 12.5 | 125 |
|---|---|---|---|---|
| $\|E\|_{L^2[0,T;L^2(\Omega)]}$ | 2.838111 | 3.125278 | 3.982163 | 4.264458 |
| $\|E - E_h\|_{L^2[0,T;L^2(\Omega)]}$ | 6.417720e-04 | 1.240301e-03 | 3.414909e-03 | 4.513999e-03 |

- *Numerical parameters:* For this example the Newton scheme always converged when the initial guess was taken to be the solution from the previous time step. Moreover, the CFL number $\tau/h$ does not significantly influence the number of iterations required. For example, with the parameters as in Figure 2, setting $\tau = 1$ (one time step) the Newton scheme converged in 6 iterations for $h \in \{1/4, 1/8, 1/16\}$.
  The regularization of the logarithm of $\det(E)$ gives rise to a consistency error of order $O(\epsilon)$. While the theory utilized a specific choice for this parameter, within the code it is only significant on the small regions where the determinant takes on the unphysical values $\det(E_h) \leq 0$, and does not significantly influence the solution or the solver. To illustrate this, with the parameters as in Figure 3 and $h = 1/16$ the errors in the deformation for different values of $\epsilon$ are:

| $\epsilon$ | 1/8 | 1/16 | 1/32 | 1/64 | 1/1000 |
|---|---|---|---|---|---|
| $\|E - E_h\|_{L^2[0,T;L^2(\Omega)]}$ | 6.652309e-03 | 2.023945e-03 | 1.285418e-03 | 1.239083e-03 | 1.241222e-03 |

Each of these runs required 64 Newton iterations (four per time step). In practice $\tau, h \nrightarrow 0$ so $\epsilon$ is fixed to be sufficiently small so that the discretization errors dominate.

### 6.2. 4:1 Contraction flow

We consider the planar flow of an Oldroyd-B fluid through the 4:1 contraction illustrated in Figure 4. The large stresses at the re-entrant corner adjacent to the very weak lip vortices challenge the fidelity of numerical schemes. In all of the examples a parabolic flow profile was specified on the inlet and outlet, the normal component of the velocity was specified on the lower boundary (center line), and homogeneous velocity boundary data specified on the rest of the boundary.

The numerical stability and convergence of the Newton scheme were very robust with respect to the Weissenberg number. The solutions shown in Figure 5 for We $= 1$, 10, and 100 (and all other parameters fixed) each took a similar number (384, 385 and 408) of Newton iterations and CPU time, and the Newton scheme converged without any subdivision of the time steps. The mesh and parameters for this example are given in Figure 6. While solutions with such a coarse mesh and large time steps at a short time do not represent a steady converged solution, 4–7 Newton iterations per time step is typical when $\tau \simeq h$. For highly refined meshes having elements much smaller than the time step, subdivision was required for certain time steps in order for the solution from the previous time step to be an adequate starting value for the Newton scheme.

To exhibit the formation of lip vortices studied in [2,7] it is necessary to significantly refine the mesh near the reentrant corner as illustrated in Figure 7. Figures 9–10 show the lip vortex that forms for different Weissenberg numbers. These figures show the streamlines in the refined area near the reentrant corner shown in Figure 7. Figure 8 shows the macroscopic streamline plot for We $= 5$, which is prototypical, and lists the rheological properties, taken from [2], and numerical parameters used for these calculations.
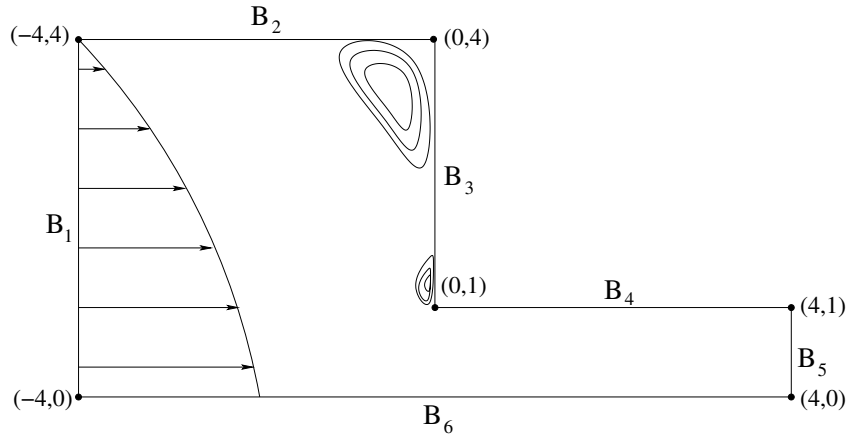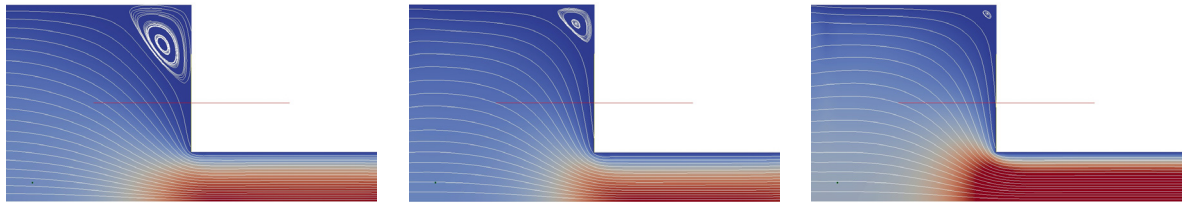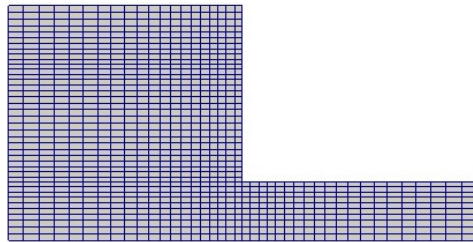
FIGURE 4. Geometry of 4:1 contraction.



FIGURE 5. Contraction flow for We = 1, 10, and 100 (streamlines over velocity magnitude).



$\mu_s = 0.1$, $\mu_p = 0.9$, $\rho = 0$, $\epsilon^2 = 10^{-6}$
$T = 2$, 128 time steps,
Implicit Euler time stepping, $(\ell = 0)$,
$\mathbb{V}_h \times \mathbb{P}_h \times \mathbb{E}_h = Q_2' \times Q_1 \times Q_1$,
(1000 elements),
Parabolic inlet and outlet profiles with unit center line velocity at the outlet.

FIGURE 6. Mesh and data for solutions in Figure 5.

Figures 9–10 clearly exhibit the dependence of the lip vortex with Weissenberg number. These flows appear to exhibit significant fine scale structure and it is not clear that steady state solutions, if they exist, are stable. The flows illustrated here were still exhibiting small fluctuations in their elastic stress consistent with elastic oscillation.

## 6.3. Flow past a disk

The drag on the flow past a cylinder is a standard benchmark problem. If $\Gamma_o \subset \partial \Omega$ is the boundary of an obstacle, the drag in a direction $e \in \mathbb{R}^d$ is given by

$$\text{Drag} \equiv \int_{\Gamma_o} Tn.e = \int_{\Gamma_o} \left( -pI + 2\mu_s D(v) + \frac{\mu_p}{\text{We}}(\alpha + \beta)(EE^\top - I) \right) n.e.$$
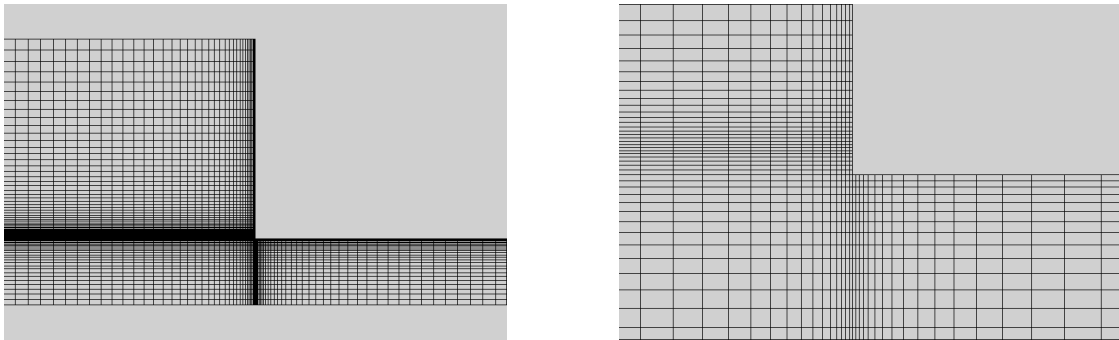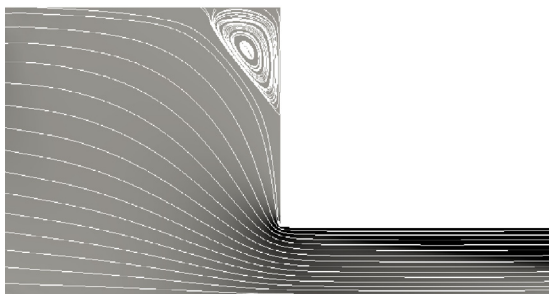
FIGURE 7. Mesh and refinement near the reentrant corner, 4200 elements.



$\mu_s = 1/9$, $\mu_p = 8/9$, $\rho = 0$, $\epsilon^2 = 10^{-6}$
$T = 8$, 128 time steps, $\tau = T/N = 0.0625$,
Implicit Euler stepping, $(\ell = 0)$,
$\mathbb{V}_h \times \mathbb{P}_h \times \mathbb{E}_h = Q_2' \times Q_1 \times Q_1$,
(2688 elements, 56,835 degrees of freedom), Parabolic
inlet and outlet profiles with center line velocity at the
outlet 3/2.

FIGURE 8. Typical streamlines and numerical and rheological data for lip vortex calculations.



FIGURE 9. 4:1 contraction with We = 0.1 and We = 1.

The numerical scheme approximates weak solutions of

$$\rho v_t + (\rho/2)(v.\nabla)v - \operatorname{div}\left(-(\rho/2)(v \otimes v) + T\right) = \rho f,$$

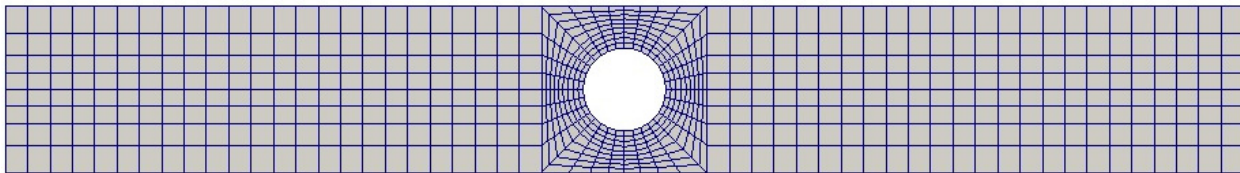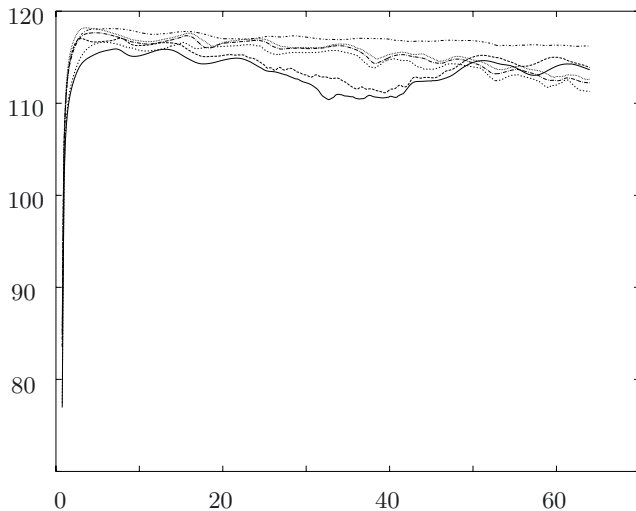FIGURE 10. 4:1 contraction with We = 5 and We = 10.



FIGURE 11. Mesh for the drag calculations.



$\mu_s = 0.51$, $\mu_p = 0.49$, $\rho = 0$, $\epsilon^2 = 10^{-6}$,
$\mathbb{V}_h \times \mathbb{P}_h \times \mathbb{E}_h = Q_2' \times Q_1 \times Q_2'$, $T = 64$ Parabolic
inlet and outlet profiles with
center line velocity at the outlet 3/2.
Dirichlet boundary data.

10 688 quadrilateral elements (top),
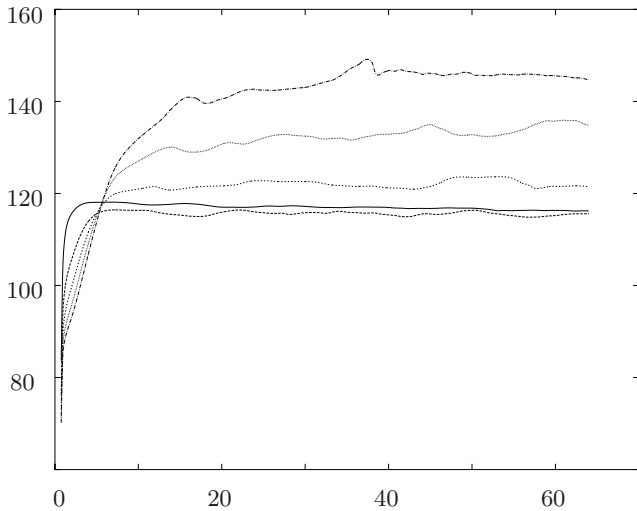2624 quadrilateral elements (middle),
672 quadrilateral elements (bottom).

FIGURE 12. Drag on cylinder verses time for We = 1/2.

so if $\phi : \Omega \to \mathbb{R}^d$ satisfies $\phi|_{\Gamma_o} = e$ and $\phi|_{\partial\Omega \setminus \Gamma_o} = 0$, integration by parts shows

$$\text{Drag} = \int_\Omega \rho \left( v_t + (1/2)(v.\nabla)v - f \right) . \phi + \left( -(\rho/2)(v \otimes v) + T \right) : \nabla\phi,$$

when $v|_{\Gamma_o} = 0$. A refinement of the mesh shown in Figure 11 was used to compute the drag as a function of time on the cylinder. The rectangular region is $[-30, 30] \times [-2, 2]$ and the cylinder has unit radius. Numerical values for the drag at various Weissenberg numbers may be found in [1, 22, 26, 29].

| We  | Drag  | Reference [1] | $\|\{\tau \mapsto \tau/2\}\|$ |
|-----|-------|---------------|-------------------------------|
| 0.5 | 116.4 | 118.8         | 8                             |
| 1.0 | 115.5 | 118.7         | 116                           |
| 1.5 | 122.5 | 126.0         | 70                            |
| 2.0 | 134.1 | 136.6         | 168                           |
| 2.5 | 145.7 | 149.1         | 450                           |

$\mu_s = 0.51$, $\mu_p = 0.49$, $\rho = 0$, $\epsilon^2 = 10^{-6}$,
$\mathbb{V}_h \times \mathbb{P}_h \times \mathbb{E}_h = Q_2' \times Q_1 \times Q_2'$, $T = 64$,
10 688 quadrilateral elements,
405 952 degrees of freedom,
2048 implicit Euler time steps ($\ell = 0$),
Parabolic inlet and outlet profiles with
center line velocity at the outlet $3/2$.
Dirichlet boundary data.

FIGURE 13. Drag on cylinder verses time, average drag over $48 \leq t \leq 64$, and number of subdivided time steps.

Figure 12 illustrates the convergence under mesh and time step refinement for this problem with the Weissenberg number fixed at We = $1/2$. The bottom two curves in the figure are for the coarsest mesh; one computed with first order time stepping $\ell = 0$, and the other with second order time stepping $\ell = 1$, each with 512 time steps. The middle three curves were computed with the mesh size halved; one with 512 and one with 2048 implicit Euler time steps, and the other with 1024 second order time steps. The upper curve was computed using the finest mesh with 2048 implicit Euler time steps. It is clear from the figure that, for this set of experiments, errors associated with (spatial) mesh resolution dominated the time stepping errors. These experiments also suggest that insufficient mesh resolution gives rise to lower values of the drag, and may give rise to excessive transient behavior; the solution with the finest mesh almost achieves a steady state.

A quantitative comparison of the drag computed with We $\in \{1/2, 1, 3/2, 2, 5/2\}$ and the results in [1] is given in Figure 13. The data in this figure is computed using the finest of the three meshes considered previously with 2048 implicit Euler time steps. In all instances the computed drag is 2–3% lower than the reported value. While this may be due to differences in the specification of the boundary data at the inlet and outlet, the results of the previous paragraph suggest that it may also be due to insufficient resolution. The final column in the table shows the number of time steps that needed to be sub–divided (at least once) in order for the Newton scheme to converge, and it is clear that, in general, the Newton scheme with maximal time step $\tau = 64/2048$ failed more as the Weisenberg number increased.

## REFERENCES

[1] A. Afonso, P. Oliveira, F. Pinho and M. Alves, The log-conformation tensor approach in the finite-volume method framework. *J. Non-Newtonian Fluid Mechanics* **157** (2009) 55–65.

[2] M.A. Alves, P.J. Oliveira and F.T. Pinho, Benchmark solutions for the flow of Oldroyd-B and PTT fluids in planar contractions. *J. Non-Newtonian Fluid Mechanics* **110** (2003) 45–75.

[3] N. Balci, B. Thomases, M. Renardy and C.R. Doering, Symmetric factorization of the conformation tensor in viscoelastic fluid models. In: XVIth International Workshop on Numerical Methods for Non-Newtonian Flows. *J. Non-Newtonian Fluid Mechanics* **166** (2011) 546–553.

[4] J.W. Barrett and S. Boyaval, Existence and approximation of a (regularized) Oldroyd-B model. *Math. Models Methods Appl. Sci.* **21** (2011) 1783–1837.

[5] S. Boyaval, Lid-driven-cavity simulations of Oldroyd-B models using free-energy-dissipative schemes, in *The eight European Conference on Numerical Mathematics and Advanced Applications*. Springer Verlag (2010) 191–198.

[6] S. Boyaval, T. Lelièvre and C. Mangoubi, Free-energy-dissipative schemes for the Oldroyd-B model. *ESAIM: M2AN* **43** (2009) 523–561.

[7]   B. Debbaut, On the inertial and extensional effects on the corner and lip vortices in a circular 4:1 abrupt contraction. *J. Non-Newtonian Fluid Mech.* **37** (1990) 281–296.

[8]   V.J. Ervin and N. Heuer, Approximation of time-dependent, viscoelastic fluid flow: Crank-Nicolson, finite element approximation. *Numer. Methods Partial Differ. Eqs.* **20** (2004) 248–283.

[9]   V.J. Ervin and N. Heuer, Approximation of time-dependent, viscoelastic fluid flow: Crank-Nicolson, finite element approximation. *Numer. Methods Partial Differ. Eqs.* **20** (2004) 248–283.

[10]  V.J. Ervin and H. Lee, Defect correction method for viscoelastic fluid flows at high Weissenberg number. *Numer. Methods Partial Differ. Eqs.* **22** (2006) 145–164.

[11]  V.J. Ervin and W.W. Miles, Approximation of time-dependent viscoelastic fluid flow: SUPG approximation. *SIAM J. Numer. Anal.* **41** (2003) 457–486.

[12]  R. Fattal, M.A. Hulsen and R. Kupferman, Flow of viscoelastic fluids past a cylinder at high weissenberg number: Stabilized simulations using matrix logarithms. *J. Non-Newtonian Fluid Mech.* **127** (2005) s27–39.

[13]  R. Fattal and R. Kupferman, Constitutive laws for the matrix-logarithm of the conformation tensor. *J. Non-Newtonian Fluid Mech.* (2004) 281–285.

[14]  R. Fattal and R. Kupferman, Time-dependent simulation of viscoelastic flows at high weissenberg number using the log-conformation representations. *J. Non-Newtonian Fluid Mech.* (2005) 23–37.

[15]  C. Guillopé and J.-C. Saut, Mathematical problems arising in differential models for viscoelastic fluids, in *Mathematical topics in fluid mechanics (Lisbon, 1991)*. Vol. 274 of *Pitman Res. Notes Math. Ser.* Longman Sci. Tech., Harlow (1992) 64–92.

[16]  M.E. Gurtin, An introduction to continuum mechanics, vol. 158 of *Mathematics in Science and Engineering*. Academic Press Inc. [Harcourt Brace Jovanovich Publishers], New York (1981).

[17]  E. Hairer, C. Lubich and G. Wanner, Geometric numerical integration, in Structure-preserving algorithms for ordinary differential equations, vol. 31 of *Springer Series in Computational Mathematics*. Springer-Verlag, Berlin (2002).

[18]  L. He and P. Zhang, L2 decay of solutions to micro-macro model for polymeric fluids near equilibrium. *SIAM J. Math. Anal.* (2009) 1905–1922.

[19]  W.J. Hrusa, M. Renardy and J.A. Nohel, Mathematical problems in viscoelasticity, vol. 35 of *Pitman Monographs and Surveys in Pure and Applied Mathematics*. Longman Scientific & Technical, Harlow (1987).

[20]  G.B. Jeffery, The motion of ellipsoidal particles immersed in a viscous fluid. *Proc. R. Soc. London* **102** (1922) 161–179.

[21]  M.W. Johnson Jr and D. Segalman, A model for viscoelastic fluid behavior which allows non-affine deformation. *J. Non-Newtonian Fluid Mech.* **2** (1977) 255–270.

[22]  Y.-J. Lee, J. Xu and C.-S. Zhang, Stable Finite Element Discretizations for Viscoelastic Flow Models, in *Numerical Methods for Non-Newtonian Fluids*, edited by R. Glowinski and J. Xu. Vol. 16 of *Handbook of Numerical Analysis*. Elsevier (2011) 371–432.

[23]  F.-H. Lin, C. Liu and P. Zhang, On hydrodynamics of viscoelastic fluids. *Comm. Pure Appl. Math.* **58** (2005) 1437–1471.

[24]  P.L. Lions and N. Masmoudi, Global solutions for some Oldroyd models of non-Newtonian flows. *Chinese Ann. Math. Ser. B* **21** (2000) 131–146.

[25]  A. Lozinski and R.G. Owens, An energy estimate for the Oldroyd B model: theory and applications. *J. Non-Newtonian Fluid Mech.* **112** (2003) 161–176.

[26]  R.G. Owens and T.N. Phillips, Computational rheology. Imperial College Press, London (2002).

[27]  M. Renardy, Mathematical analysis of viscoelastic flows. Vol. 73 of *CBMS-NSF Regional Conference Series in Applied Mathematics*. Society for Industrial and Applied Mathematics (SIAM), Philadelphia, PA (2000).

[28]  R.E. Showalter, Monotone operators in Banach space and nonlinear partial differential equations. American Mathematical Society, Providence, RI (1997). Available at: http://www.ams.org/online_bks/surv49/

[29]  J. Sun, M. Smith, R. Armstrong and R. Brown, Finite element method for viscoelastic flows based on the discrete adaptive viscoelastic stress splitting and the discontinuous Galerkin method: DAVSS-G/DG. *J. Non-Newtonian Fluid Mech.* **86** (1999) 281–307.

[30]  V. Thomee, Galerkin Finite Element Methods for Parabolic Problems. Vol. 1054 of *Lect. Notes Math.* Springer (1984).

[31]  N.J. Walkington, Numerical approximation of nematic liquid crystal flows governed by the Ericksen-Leslie equations. *ESAIM: M2AN* **45** (2011) 523–540.

[32]  K. Yosida, Functional Analysis. Vol. 123 of *Grundlehren Math. Wiss.*, Springer Verlag (1980).